



HAL
open science

Diastolic Cardiomyopathy Secondary to Experimentally Induced Exacerbated Emphysema

Pierre-Edouard Grillet, Elodie Desplanche, Quentin Wynands, Fares Gouzi, Patrice Bideaux, Aurelie Fort, Valérie Scheuermann, Alain Lacampagne, Anne Virsolvy, Jérôme Thireau, et al.

► **To cite this version:**

Pierre-Edouard Grillet, Elodie Desplanche, Quentin Wynands, Fares Gouzi, Patrice Bideaux, et al.. Diastolic Cardiomyopathy Secondary to Experimentally Induced Exacerbated Emphysema. American Journal of Respiratory Cell and Molecular Biology, 2023, 69 (2), 10.1165/rcmb.2022-0382OC . hal-04094438

HAL Id: hal-04094438

<https://hal.science/hal-04094438>

Submitted on 18 Oct 2023

HAL is a multi-disciplinary open access archive for the deposit and dissemination of scientific research documents, whether they are published or not. The documents may come from teaching and research institutions in France or abroad, or from public or private research centers.

L'archive ouverte pluridisciplinaire **HAL**, est destinée au dépôt et à la diffusion de documents scientifiques de niveau recherche, publiés ou non, émanant des établissements d'enseignement et de recherche français ou étrangers, des laboratoires publics ou privés.

Diastolic cardiomyopathy secondary to experimentally induced exacerbated emphysema

Pierre-Edouard Grillet PharmD,PhD^a, Elodie Desplanche MSc^a, Quentin Wynands MSc^{a,b}, Fares Gouzi MD,PhD^{a,c}, Patrice Bideaux^a, Aurelie Fort PhD^b, Valérie Scheuermann MSc^a, Alain Lacampagne PhD^a, Anne Virsolvy PhD^a, Jérôme Thireau PhD^a, Pieter de Tombe PhD^a, Arnaud Bourdin MD,PhD^{a,b*}, Olivier Cazorla PhD^{a*}

*Equal contribution

^a PhyMedExp INSERM, CNRS, Université de Montpellier, CHU Montpellier, France.

^b Department of Respiratory Diseases, Université de Montpellier, CHU Montpellier, Hôpital Arnaud de Villeneuve, France

^c Department of Physiology, Université de Montpellier, CHU Montpellier, France.

Short title: Exacerbated emphysema induced HFpEF

Category of manuscript: Original article

Correspondence to:

Olivier CAZORLA

PhyMedExp, Université de Montpellier, INSERM, CNRS,

CHU Arnaud de Villeneuve

34295 Montpellier, France

Phone: +33 467 41 52 44

Fax: +33 467 41 52 42

olivier.cazorla@inserm.fr

Orcid IDs : 0000-0002-5695-5020 (PEG), 0000-0001-8970-866X (FG), 0000-0003-0264-1787 (AL), 0000-0002-5819-3306 (AV), 0000-0002-1641-5142 (JT), 0000-0003-3178-0233 (PdT), 0000-0002-4645-5209 (AB), 0000-0003-0775-203X (OC)

AUTHOR CONTRIBUTION

The authors confirm contribution to the paper as follows: Conception or design of the work: OC, AB. Data collection: PEG, ED, QW, JT, AF, PB, VS. Data analysis and interpretation of results: PEG, ED, QW, JT, AF, PdT, OC. Drafting the article: PEG, PdT, OC, AB. Critical revision of the article: OC, AB, JT, AV, FG, PdT. All authors reviewed the results and approved the final version of the manuscript.

ABSTRACT

Chronic Obstructive Pulmonary Disease (COPD) is a clinical entity of increasing significance. COPD involves abnormalities of the airways and in emphysema, parenchymal pulmonary destruction. Cardiovascular disease has emerged as a significant comorbidity to COPD. Heart Failure with preserved Ejection Fraction (HFpEF) appears to be particularly associated with COPD-Emphysema. Traditional treatments have shown limited efficacy in improving COPD associated HFpEF. This lack of therapeutic efficacy highlights the need to identify potential mechanisms that link COPD-Emphysema to HFpEF. Therefore, we aimed to study the delayed cardiac physiological impacts in a rat model with acute exacerbated emphysema. Emphysema was induced by 4 weekly 4UI elastase intra-tracheal pulmonary instillations and exacerbation by one final additional LPS instillation in male Wistar rats. At 5 weeks following the LPS/elastase exposure, *in-vivo* and *ex-vivo* pulmonary and cardiac measurements were performed. Experimental exacerbated emphysema resulted in decreased pulmonary function and exercise intolerance. Histological analysis revealed parenchymal pulmonary destruction without signs of inflammation or cardiac fibrosis. *In-vivo* cardiac functional analysis revealed diastolic dysfunction and tachycardia. *Ex-vivo* analysis revealed a cellular cardiomyopathy with decreased myofilament Ca^{2+} sensitivity, cross-bridge cycling kinetics and increased adrenergic PKA-dependent phosphorylation of troponin-I. Experimental exacerbated emphysema was associated with exercise intolerance that appeared to be secondary increased β -adrenergic tone and subsequent cardiac myofilament dysfunction. A β 1-receptor antagonist treatment (bisoprolol) started 24h post ELA-LPS instillation prevented *in-vivo* and *ex-vivo* diastolic dysfunction. These results suggest that novel treatment strategies targeted to the cardiac myofilament may be beneficial to combat exacerbated emphysema associated HFpEF.

Keywords: **elastase, cardiac myofilaments, calcium, COPD, HFpEF.**

Translational perspectives

- Exacerbated emphysema animal model is suitable to mimic the physiopathology of COPD patients, especially cardiac alterations consisting in diastolic heart failure with preserved ejection fraction.
- *Ex-vivo* analysis revealed a cellular cardiomyopathy probably caused by increased circulating catecholamines and chronotropic incompetence.
- β 1-blocker therapy appears to be relevant to reduce diastolic dysfunction, chronotropic incompetence and cellular changes.
- Further investigation is warranted to validate the mechanism by which selective β 1 receptor antagonism reduce or delay the risk of cardiomyopathy in COPD patients.

Abbreviation list:

AMP: adenosine mono-phosphate
COPD: chronic obstructive pulmonary disease
ECG: electrocardiogram
HFpEF: heart failure with preserved ejection fraction
LVEF: left ventricular ejection fraction
LPS: lipopolysaccharide
PKA: protein kinase A
SL: sarcomere length
TAPSE: tricuspid annular plane systolic excursion
TDI: tissue Doppler imaging

INTRODUCTION

Chronic Obstructive Pulmonary Disease (COPD) is a clinical entity of increasing significance towards morbidity and mortality worldwide ^{1,2}. COPD involves abnormalities of the airways and, in emphysema, parenchymal pulmonary destruction. Emphysema may lead to pulmonary hyperinflation as a consequence of blunted lung elastic recoil and gas trapping of pulmonary air ¹. In addition, cardiovascular disease has emerged as a significant comorbidity to COPD, irrespective of shared risk factors such as cigarette smoking, pollution, sedentary lifestyle and ageing ³. Moreover, large cohort studies support the notion of a crosstalk between COPD-Emphysema and cardiovascular disease ^{4,5}.

Diastolic heart failure (HF), also termed heart failure with preserved ejection fraction (HFpEF), appears to be particularly associated with severe COPD-Emphysema ^{4,6}. Conversely, prognosis in HFpEF is worsened in the presence of COPD ⁵. Treatments such as inhaled corticosteroids, statins, and diuretics have shown limited efficacy in improving COPD associated HFpEF ⁷, consistent with the observation that traditional therapeutic strategies aimed to combat systolic heart failure have also been largely unsuccessful to treat HFpEF ⁸. Diastolic dysfunction, the hallmark of HFpEF, has been attributed to three main cellular mechanisms: cardiac fibrosis with increased tissue stiffness, deranged calcium homeostasis, and post-translational modifications of myofilament's proteins ⁹. However, the contribution of COPD in these pathways is yet to be determined. Consequently, the lack of therapeutic efficacy to ameliorate HFpEF, particularly in COPD patients, highlights the need to identify potential cellular mechanisms that link COPD-Emphysema to HFpEF ^{10,11}.

Few studies have examined mechanisms that may underlie development of HFpEF in COPD-Emphysema patients. One possibility is the impact of pulmonary hyperinflation on cardiac preload *via* a mechanical constraint imposed onto the heart. Indeed, surgically ¹² or pharmacologically ¹³ induced lung deflation has been shown to improve cardiac function. In addition, increased pulmonary vascular resistance may cause yet another extra-cardiac limitation to cardiac function in COPD ¹⁴. However, intra-cardiac causes of cardiac dysfunction in COPD-Emphysema cannot be excluded, but are yet to be examined.

COPD patients display increased vulnerability to pulmonary virus and/or bacterial infections that can induce acute exacerbations of the disease and systemic inflammation¹⁵. In the context of COPD, the delayed impact of transient pulmonary inflammation in presence of emphysema on cardiac function has not been examined in detail. Animal models reproducing exacerbated emphysema associated with cardiac dysfunction are essential to determine cellular and molecular mechanisms underlying the syndrome. Since the 1970s several experimental models have used single-dose¹⁶ treatment or more recently multiple-dose elastase treatment to induce emphysema. Among these, some studies have explored cardiac alterations, especially on the right side and pulmonary artery. Indeed, right heart dilatation and hypertrophy correlated to emphysema¹⁷, pulmonary artery remodeling and hypoxic hyperactivity¹⁸, and echocardiographic documented alterations of pulmonary artery function (PAT/PET)¹⁹ have been described in elastase-induced emphysema rat models. Lately these experimental models have been combined with lipopolysaccharide (LPS) treatment to mimic acute pulmonary infection/exacerbation. Accordingly, in the present study we adapted these mouse²⁰ and rat²¹ models to study the delayed impact of transient pulmonary inflammation in presence of emphysema, on cardiac function. We used a multi-dose treatment exacerbated emphysema model, that is based on four weekly intra-tracheal pulmonary instillations of elastase, followed by a final elastase instillation combined with LPS. A significant finding of our study is exacerbated emphysema induced diastolic heart failure that may be the result of molecular cellular alterations of cardiac myocytes, and in particular the cardiac myofilament.

METHODS

An expanded Methods section is available in the on-line supplement.

Animal Model

All investigations conformed to European Parliament Directive 2010/63/EU and were approved by the local ethics committee (APAFIS#13133-2018012212031585v2). Experimental emphysema was induced in seven-week-old sedated male rats (1% isoflurane) by intra-tracheal instillation of pancreatic porcine elastase (ELA, 4 units/200 μ L saline solution, Sigma-Aldrich, France) once a week for four weeks (Fig. 1A). To mimic COPD exacerbations related

to recurrent pulmonary infections, rats received with the last ELA instillation, a single dose of LPS (E.coli O55:B5, 2.5mg/kg, Sigma-Aldrich, France). Control animals were handled identically but did not receive any instillation. Next, animals were kept for 5 weeks following the last pulmonary instillation to allow for examination of the functional impacts of exacerbation-emphysema that remained after the acute inflammatory phase post ELA-LPS. In addition, a subgroup of animals was treated with a β_1 -receptor antagonist (2.5mg/kg/day in drinking water, bisoprolol hemifumarate, MedChemExpress, USA) starting 24h *post* ELA-LPS instillation (Fig. 1A). Rats were euthanized with sodium pentobarbital overdose (140mg/kg, *i.p.*).

In-vivo respiratory and cardiac functions and exercise tolerance

In-vivo physiological functions were tested one day before sacrifice including:

Respiratory function using a whole-body plethysmograph in awake animals as previously described²². Parameters included respiratory rate, minute volume, peak inspiratory flow, and peak expiratory flow.

Maximum Oxygen consumption, assessed by an incremental exercise test on a metabolic treadmill, as well as VO_{2max} and maximum running distance.

Cardiovascular function, explored by echocardiography on anesthetized animals (Isoflurane, 2.5–3.5%) as previously described²³ and non-invasive systemic pressure by tail-cuff after familiarization of animals to the procedure.

Electrocardiograms (ECG), using telemetric transmitter for 24h during normal activity in the cage as previously described²⁴. For dobutamine testing (2mg/kg, *i.p.*), ECGs were recorded 4 hours pre- and 4 hours post-injection.

Histological characterization of emphysema, fibrosis and inflammation

For histological analysis, explanted lungs were inflated to 25cm H₂O pressure with 4% formol by means of tracheal cannulation, and then immersed in 4%-formol. Mean linear intercept was measured on lung tissue sections as previously described²⁵. The heart was either directly immersed in 4%-formol for histology, or rapidly frozen with liquid N₂ cooled clamps followed by -80°C storage for biochemistry or myofilament studies. Collagen content was evaluated on cardiac tissue sections using picosirius red staining.

Western-Blot analysis

Cyclic AMP dependent protein kinase (PKA) dependent myocardial protein phosphorylation was determined by Western-Blot analysis as previously described²⁶. Frozen LV tissue was pulverized on dry-ice, solubilized in non-reducing Laemmli buffer followed by SDS-PAGE and Western-Blot. Phosphorylation levels were expressed relative to total protein content.

Single cardiomyocyte analysis

Membrane intact cardiomyocytes were isolated from the heart by enzymatic digestion as previously described²⁴. To analyze cell shortening and Ca²⁺ homeostasis, signals of sarcomere length (SL) and Indo-1 ratiometric fluorescent Ca²⁺ indicator were recorded at 1 Hz (IonOptix system).

Cardiac myofilament function was assessed in permeabilized cardiomyocytes obtained from the frozen samples as previously described²⁷. Parameters calculated included maximum Ca²⁺ induced myofilament force and Ca²⁺ sensitivity.

Statistical analysis

Data are presented as mean±SEM or as median with total distribution and 25 – 50% interquartile. Differences were assessed either by the Student's *t*-test or by the Mann Whitney's rank test whenever the data distribution was found not to be Gaussian as determined by the Shapiro-Wilk's normality test (GraphPad Prism). Analysis of differences for three groups was assessed by one-way ANOVA analysis followed by Bonferonni's multiple-comparisons test or Kruskal-Wallis test with Dunn's correction for the multiple comparison post hoc test. *p*<0.05 was considered significant.

RESULTS

Exacerbated emphysema rat model

The experimental protocol employed to induce exacerbated emphysema is schematically illustrated in Figure 1A. Five weeks following elastase and LPS tracheal instillations, *post-mortem* lung tissue histological analysis

revealed significant parenchymal alveolar destruction as presented in Figure 1B. The resulting alveolar enlargement, as quantified by the mean linear intercept dimension parameter, was increased by ~50% in the emphysema group. In addition, we found no evidence of ELA-LPS induced major chronic inflammation measured by pulmonary immunohistochemistry or systemic plasma cytokine and chemokine analysis (cf. Supplemental Figure 1).

In-vivo whole-body plethysmography confirmed the development of exacerbated emphysema as illustrated in Figure 1. In particular, peak expiratory flow was significantly reduced in the ELA-LPS group (Fig. 1D). Peak inspiratory flow, in contrast, was not impacted by ELA-LPS treatment (Fig. 1C), as were other parameters such as respiratory rate and minute volume (cf. Supplemental Table 1).

Maximal oxygen uptake (VO_{2max}), as measured during an incremental metabolic treadmill exercise test, was significantly reduced in the ELA-LPS group (Fig. 1E), as was the maximum running distance (Fig. 1F).

Overall, these *in-vivo* functional physiological data are consistent with presence of exacerbated emphysema and a concomitant reduction in global exercise capacity.

Functional signs of HFpEF

At the conclusion of the five-week incubation period, ELA-LPS animals displayed a ~20% increase in heart rate as measured by ECG telemetry (cf. Supplemental Table 2). Mean arterial pressure assessed by the tail-cuff method was also significantly increased in ELA-LPS animals (119.9 ± 2.4 mmHg, n=15) compared to control animals (107.2 ± 1.8 mmHg, n=11). Echocardiographic evaluation was next performed in lightly sedated (isoflurane) animals. Since heart rate is a confounding factor in echocardiography, the isoflurane dosage was adjusted to achieve similar heart rates (~350 bpm) in control and ELA-LPS animals. Echocardiographic assessed parameters included M-mode chamber dimensions (Fig. 2A), mitral-flow Doppler (Fig. 2B), and mitral-tissue Doppler (Fig. 2C). A complete summary of the acquired measurements can be found in the supplementary data section (cf. Supplemental Table 3). ELA-LPS treatment resulted in unchanged left ventricular ejection fraction (LVEF%; Fig. 2A), but increased E/A (Fig. 2B) and E/e' (Fig. 2C) ratios, as well as a ~10% reduction in cardiac output (cf. supplement Table 3). There was no apparent echocardiographic alteration in right ventricular systolic function as indexed by TAPSE and S tricuspid wave velocity (Supplemental Table 3).

These *in-vivo* cardiac functional findings are consistent with diastolic dysfunction resulting in the syndrome of HFpEF²⁸, a condition commonly seen in COPD-Emphysema patients.

Myocardial hypertrophy without fibrosis

Post-mortem histological analysis revealed no sign of increased myocardial or perivascular fibrosis in the ELA-LPS group (Fig. 3A). Cardiac hypertrophy was detected in ELA-LPS treated animals as indexed by an increase in cardiac mass (Fig. 3B) and cardiac myocyte cell surface area (Fig. 3C). These findings indicate left ventricular hypertrophy in the absence of cardiac fibrosis.

Altered cardiac myocyte function

The HFpEF syndrome is due to impeded diastolic ventricular filling. Since the histological analysis excluded contribution of cardiac fibrosis in the stiffening of the heart (Fig. 3A), we next focused on the potential role of cardiac myocyte function in the observed syndrome. Membrane intact cardiac myocytes were isolated from Ctrl and ELA-LPS animals and *ex-vivo* functional tests were performed using an IonOptix cell system. The results are presented in Figure 4. Measurements on membrane intact and unloaded isolated cardiac myocytes revealed enhanced cellular Ca²⁺ homeostasis in the ELA-LPS group. This was witnessed by increases in the basal level of [Ca²⁺] (Fig. 4B), Ca²⁺ transient (Fig. 4C), and Ca²⁺ reuptake rate (Fig. 4D). The alteration in cellular Ca²⁺ homeostasis was accompanied by cellular SL lusitropy (kinetics) (Fig. 4H), but not by enhanced SL shortening (Fig. 4G) or reduction in basal SL (Fig. 4F). These results may be indicative of increased adrenergic tone in exacerbated emphysema animals. However, the enhanced Ca²⁺ homeostasis did not affect cellular contractility as indexed by the magnitude of SL shortening. Hence, these cellular excitation-contraction results do not fully explain the *in-vivo* HFpEF syndrome that is characterized, among other factors, by impaired cardiac relaxation.

Altered cardiac myofilament function

The membrane intact isolated cardiac myocyte measurements summarized above take place, by design, under unloaded conditions where sarcomeres operate at lengths well below those encountered *in-vivo* and, moreover, with minimal myofilament force development. Hence, such measurements report, predominantly, on cardiac cellular Ca²⁺ homeostasis, but not on *in-vivo* cellular contractile function. To overcome this limitation, we additionally directly

examined myofilament function in isolated attached and force developing permeabilized (skinned) cardiac myocytes as presented in Figure 5. Skinned myocytes were exposed to varying levels of activating $[Ca^{2+}]$ (Fig. 5A). Maximum $[Ca^{2+}]$ activated force generating capacity was slightly increased in the ELA-LPS group (Fig. 5B). In addition, myofilament Ca^{2+} sensitivity, as indexed by pCa_{50} , was significantly blunted in exacerbated emphysema animals (Fig. 5C). Another important parameter of myofilament function is the rate of cross-bridge cycling, which we indexed here by K_{tr} . The K_{tr} parameter reflects the rate of force redevelopment following a rapidly imposed release-re-stretch maneuver as illustrated in Fig. 5D. ELA-LPS skinned myocytes displayed a significant slowing of myofilament cross-bridge cycling (Fig. 5E). Taken together, these myofilament measurements indicate a blunting of myofilament Ca^{2+} activating properties and slowing of cross-bridge cycling that is expected to contribute to a reduced cardiac relaxation rate and a resulting diastolic dysfunction *in-vivo*.

β-adrenergic pathways

Our cellular Ca^{2+} homeostasis results (Fig. 4) are suggestive of increased β-adrenergic tone in **exacerbated emphysema**. This notion was confirmed by a blunted *in-vivo* response to dobutamine infusion (Fig. 6A) in the ELA-LPS group indicative of reduced adrenergic reserve. In addition, the levels of cardiac Troponin-I phosphorylation at Serines 22/23 increased in ELA-LPS animals. These residues form the down-stream β-adrenergic pathway targets for this contractile protein (Fig. 6B). Increased circulating catecholamine levels are a common finding in heart failure. Moreover, pharmacological treatment with β-adrenergic receptor antagonists has been shown to be of benefit, at least in systolic heart failure. To evaluate whether β-blockers may be beneficial, ELA-LPS rats were treated with Bisoprolol, a specific β₁-receptor antagonist, for 5-weeks, 1 day following exacerbated emphysema induction (Fig. 1A). *In-vivo* evaluation by echocardiography revealed a reversal of cardiac diastolic dysfunction (Fig. 6C), a recovery of the blunted dobutamine stress-test (Fig. 6A) and a **statistical trend towards a reduction** of PKA-induced phosphorylation of Troponin-I (Fig. 6B). Moreover, *in-vivo* cardiac contractility was not affected as demonstrated by a maintained LVEF (Fig. 6D).

Similar findings were observed at the cellular level, as illustrated in Figure 7. β-blocker treatment impacted cardiac calcium homeostasis by reducing the amplitude of calcium released (Fig. 7C), slowing of calcium reuptake

(Fig. 7D) and a higher basal calcium level (Fig. 7B). These are alterations that are consistent with β -blocker treatment effects. That is, many of the membrane-intact cellular contractility and Ca^{2+} homeostasis parameters reversed, at least partially, to values observed in the control group. Moreover, the depressed myofilament cross-bridge cycling rate, as indexed by the K_{tr} parameter (Fig. 7G), reverted to values seen in control skinned myocytes.

Overall, these *in-vivo* and *ex-vivo* data suggest that β_1 -specific receptor antagonists may be beneficial to combat HFpEF in COPD-exacerbated emphysema.

DISCUSSION

Experimental exacerbated emphysema

The first aim of this study was to assess the relevance of an experimental exacerbated-emphysema rat model for exploring cardiac dysfunction, as seen in COPD patients. Our experiments showed that multiple orotracheal instillations of elastase followed by a single final simultaneous instillation of LPS, and subsequent 5-week incubation period, is effective in inducing pathologies that resemble those seen in COPD-exacerbated emphysema: alveolar parenchymal destruction, alveolar enlargement, airflow obstruction, and exercise intolerance. Of note, FEV₁, a common clinical COPD index, is not accessible in animals. Importantly, our experimental model, by design, exhibits only the chronic impact of inflammation due to LPS exacerbation, as evidenced by the lack of circulating cytokines and pulmonary white blood cells. This is the first time this type of elastase induced emphysema and exacerbation rat model is explored in depth in terms of the delayed impacts on cardiac function; that is, previous studies focused either on events during the acute phases (within hours) following elastase or LPS treatment,^{21,29,30} or only on pulmonary pathophysiology³¹.

Five weeks following the last elastase-LPS instillation, we found chronic tachycardia, exercise intolerance, increased β -adrenergic tone, reduced cardiac output, and cardiac hypertrophy. Most importantly, we also found signs of LV diastolic dysfunction, but preserved cardiac contractility by echocardiography. These are the well-established clinical signs of diastolic heart failure as specified in pre-clinical guidelines²⁸. Thus, we succeeded in creating an exacerbated emphysema small rodent model associated with HFpEF.

We found no evidence of right ventricular dysfunction by echocardiography, in contrast to previous acute studies^{21,32}. This could be related to acute versus chronic impacts. Moreover, we deliberately used relatively low doses of elastase to allow for study of the chronic impacts of emphysema. Nevertheless, it is possible that subtle alterations in RV function were below the detection limit of right-sided echocardiography in rats and this would be the scope of further explorations of this experimental model. The cardiac phenotype was explored 5 weeks after the last instillation to better fit with the existing literature of the ELA-LPS model³³. It will be interesting to explore cardiac function later after this period to verify if the heart decompensates on both sides.

A previous publication classified the level of increase in mean linear intercept to the severity of emphysema²⁵. According to their classification, an increase of 54% of the mean linear intercept of ELA-LPS animals suggests that our animals exhibited moderate to severe emphysema. Emphysema has been shown to be accompanied by lung hyperinflation that could induce “mechanical” diastolic dysfunction, mimicking a gaseous tamponade^{6,12}, either caused by reduced LV filling and, thus, reduced myocardial preload³⁴, or caused by elevation of pulmonary arterial pressure/resistance¹⁸ or right ventricle pressure³⁵. De Oliveira *et al*²¹, employing a similar rat model of emphysema, showed pulmonary hyperinflation induced by emphysema as assessed by micro-computed tomography. Thus, our experimental animals most likely exhibited some pulmonary hyperinflation, and this still needs to be quantified. Therefore, pulmonary vessels³⁴ and atrial abnormalities could also play a role in the current exacerbated emphysema experimental animal model that needs to be further explored.

Inflammation and oxidative stress are major mechanisms known to contribute to COPD and HFpEF that may affect cardiac function. We did not find significant signs of circulating determinant of inflammation 5 weeks following induction of exacerbated emphysema, but for increased circulating IL-13 levels and a tendency for increased IL-6, IL-4 and IL-1B that did not reach statistical significance ($p=0.064$, $p=0.076$ and $p=0.21$, respectively). Oliveira *et al*²¹ used a similar rat model but followed a different protocol: emphysema induced (4xELA at 2UI), 5 week incubation, followed by a final LPS instillation, and analysis after 24h. They observed in the lungs an elevation of the levels of cytokine-induced neutrophil chemoattractant-1, interleukin (IL)-1 β , tumor necrosis factor- α , IL-6, and vascular endothelial growth factor in lung tissue, collagen fiber deposition in alveolar septa, airways, and pulmonary vessel walls, and increased dynamic lung elastance. In their study, inflammation in the lungs was associated with depressed LV systolic cardiac function as indexed by diminished LVEF. LV diastolic function, however, was not assessed. In contrast, we did not find significant modifications in pulmonary white blood cell content. However, it should be noted

that in our experimental model, measurements were made well beyond the acute phase of inflammation, most likely after the “inflammation storm” induced by LPS instillation. Hence, the absence of elevated pulmonary white blood cells in lungs and plasma cytokines does not exclude inflammation induced cardiac dysfunction in this model. This could be explored by studying the extent of inflammation and cardiac dysfunction between the acute phase (LPS instillation) and the end of the protocol (*i.e.* 5 weeks incubation).

Altered cardiac myocyte function in exacerbated emphysema.

We did not find evidence for increased myocardial collagen deposits nor cardiac fibrosis. This absence of fibrosis, although uncommon, has already been found in other experimental HFpEF models³⁶ and could be due to the relatively young age of the animals that we studied. We observed a modest but significant decrease in collagen content in ELA-LPS animals. The collagen content is calculated as the ratio of collagen area to collagen area plus myocyte area. Since the cell surface of the myocytes increased by 15% this could affect the relative content of collagen and may be responsible for the apparent relative decrease of collagen content. Therefore, it is unlikely that cardiac fibrosis underlies the diastolic dysfunction seen in our experimental exacerbated emphysema rat model.

ELA-LPS treatment resulted in enhanced cellular Ca^{2+} homeostasis closely resembling features of cardiac β -adrenergic stimulation such as increased basal cellular $[\text{Ca}^{2+}]$ and magnitude of the Ca^{2+} transient, concomitant with accelerated Ca^{2+} kinetics. Indeed, evidence for increased circulating catecholamines included chronic tachycardia, a blunted dobutamine chronotropic response, and contractile protein Troponin-I PKA mediated phosphorylation. The cellular Ca^{2+} homeostasis alterations were mirrored in SL mechanical parameters, with the notable exception of the extent of SL shortening. The latter is the cellular equivalent of whole heart ejection fraction and, as such, indicates that despite the increased Ca^{2+} transient, cellular contractility was not affected. This implicates modification of the cardiac myofilament contractile protein's response to activating Ca^{2+} . Indeed, direct examination of cardiac myofilament properties employing permeabilized cardiac myocytes confirmed this hypothesis. That is, both myofilament Ca^{2+} sensitivity and cross-bridge cycling rate were found to be reduced in the ELA-LPS group. While, a decrease in myofilament Ca^{2+} sensitivity following β -adrenergic stimulation is well established³⁷, a decrease in the cross-bridge cycling rate is not³⁸. This is likely the result of cardiac pathology, e.g. left ventricular hypertrophy secondary to chronic adrenergic stimulation. Our results suggest that novel treatment strategies targeting the cardiac myofilament may be of particular benefit in COPD-Emphysema.

β-adrenergic pathways

The finding of evidence for increased levels of circulating catecholamines in exacerbated emphysema animals prompted us to explore possible benefits of chronic β-antagonist therapy. Chronic β-adrenergic stimulation has been shown to induce HFpEF in experimental animal models³⁹. There is an extensive literature focused on β-blocker therapy in COPD and/or HFpEF patients with meta-analysis and registry^{40,41}, or randomized controlled clinical trials^{42,43}. However, clinical trials have mainly focused on safety outcomes concerning pulmonary function and exacerbation risk, or were designed to test acute exacerbation treatment scenarios⁴⁴. Indeed, to date persistent controversies remain regarding β-blocker therapy use in COPD patients⁴⁵.

In the current study, we demonstrated reversal of both HFpEF signs and cellular alterations in response to chronic β₁-specific receptor antagonist treatment in ELA-LPS animals. The cellular and molecular mechanisms underlying this beneficial impact are not entirely clear but may relate to blunting of chronic cellular Ca²⁺ homeostasis “overload” leading to the syndrome of diastolic heart failure. Clarification of these mechanisms will require further investigations.

Limitations

It should be noted that our model explores the impact of chronic β₁-blocker therapy in the absence of one of the main therapeutic approaches employed in COPD, β₂ agonists. These agents could exacerbate detrimental outcomes in an adrenergic overstimulation environment such as the one we described for our model.

Like most, if not all, previous published studies on emphysema we have used only male rats to avoid physiological sex differences including hormonal variations. In many disease models, males are more sensitive to stress due to the absence of female hormones (*i.e.* cardiotoxicity of anthracyclines⁴⁶). This seems to be also the case for emphysema, since the experimental induction of emphysema in developing rats was prevented by daily injections of progesterone or medroxyprogesterone⁴⁷. Sex impact in patients and experimental animal models have been investigated mostly with regard to cigarette smoking, where the sex appears to affect cigarette smoke detoxification by cytochrome P450. Accordingly, we cannot exclude the impact of sex on the outcomes of the current investigation.

The chronic cigarette smoke exposure model has been considered as a major component of COPD natural history and the “gold standard” for the animal experimental model of COPD. However, reported clinical studies highlight the existence of many non-smokers COPD patients, especially in the young⁴⁸. Moreover, cigarette smoke exposure in rodent models have shown limited pathophysiological impacts, equivalent to mild or moderate COPD GOLD stages I and II^{49,50}. In the context of our study, therefore it would be of great interest to evaluate LV dysfunction in a combined model with cigarette smoke and elastase exposure in the future.

The study of TnI phosphorylation in the group treated by β -blocker may have been insufficiently powered to achieve statistical significance. Anyway, the trend supports our hypothesis still.

Conclusions

Experimental exacerbation-emphysema was associated with exercise intolerance and diastolic heart failure due to increased β -adrenergic tone and subsequent cardiac cellular and myofilament dysfunction. Chronic selective β_1 receptor antagonist treatment reversed many of these impacts. Our results suggest that novel treatment strategies involving selective β -receptor subtypes and targeted to the cardiac myofilament may be beneficial to combat exacerbated emphysema associated HFpEF.

Data availability statement: The data underlying this article will be shared on reasonable request to the corresponding author.

Funding: This work was supported by the Fédération Française de Cardiologie to AB (#R20012FF).

Competing interests: The authors have no disclosures to declare related to this paper, except for AB who has, within the two last years, received personal fees from GlaxoSmithKline, Regeneron, Chiesi, Teva, Boehringer Ingelheim; personal fees and other from AstraZeneca and Novartis.

Acknowledgments: The authors thank Laurie Albuquerque from the Lab animal facility, the Imagerie du Petit Animal de Montpellier (IPAM) for access to high-resolution ultrasound and Montpellier Ressources Imagerie (MRI, BioCampus, CNRS) for access to the slide scanner. We also want to thank I. Serre and the Department of Pathology

of the Montpellier University Hospital for access to the histologic platform and S. Lehmann and C. Hirtz for accessing to the PPC platform (IRMB, Montpellier, France).

REFERENCES

- 428 1. Global Initiative for Chronic Obstructive Lung Disease. Global Initiative for Chronic
429 Obstructive Lung Disease Report 2020<http://goldcopd.org/> (2 April 2020)
- 430 2. Soriano JB, Abajobir AA, Abate KH, Abera SF, Agrawal A, Ahmed MB, Aichour AN,
431 Aichour I, Aichour MTE, Alam K, Alam N, Alkaabi JM, Al-Maskari F, Alvis-Guzman N,
432 Amberbir A, Amoako YA, Ansha MG, Antó JM, Asayesh H, Atey TM, Avokpaho EFGA,
433 Barac A, Basu S, Bedi N, Bensenor IM, Berhane A, Beyene AS, Bhutta ZA, Biryukov S,
434 Boneya DJ, Brauer M, Carpenter DO, Casey D, Christopher DJ, Dandona L, Dandona R,
435 Dharmaratne SD, Do HP, Fischer F, Geleto A, Ghoshal AG, Gillum RF, Ginawi IAM,
436 Gupta V, Hay SI, Hedayati MT, Horita N, Hosgood HD, Jakovljevic M (Michael) B,
437 James SL, Jonas JB, Kasaeian A, Khader YS, Khalil IA, Khan EA, Khang YH,
438 Khubchandani J, Knibbs LD, Kosen S, Koul PA, Kumar GA, Leshargie CT, Liang X,
439 Razek HMA El, Majeed A, Malta DC, Manhertz T, Marquez N, Mehari A, Mensah GA,
440 Miller TR, Mohammad KA, Mohammed KE, Mohammed S, Mokdad AH, Naghavi M,
441 Nguyen CT, Nguyen G, Nguyen Q Le, Nguyen TH, Ningrum DNA, Nong VM, Obi JI,
442 Odeyemi YE, Ogbo FA, Oren E, PA M, Park EK, Patton GC, Paulson K, Qorbani M,
443 Quansah R, Rafay A, Rahman MHU, Rai RK, Rawaf S, Reinig N, Safiri S, Sarmiento-
444 Suarez R, Sartorius B, Savic M, Sawhney M, Shigematsu M, Smith M, Tadese F,
445 Thurston GD, Topor-Madry R, Tran BX, Ukwaja KN, Boven JFM van, Vlassov VV,
446 Vollset SE, Wan X, Werdecker A, Hanson SW, Yano Y, Yimam HH, Yonemoto N, Yu C,
447 Zaidi Z, Sayed Zaki M El, Murray CJL, Vos T. Global, regional, and national deaths,
448 prevalence, disability-adjusted life years, and years lived with disability for chronic

- 449 obstructive pulmonary disease and asthma, 1990–2015: a systematic analysis for the
450 Global Burden of Disease Study 2015. *Lancet Respir Med* 2017;**5**:691–706.
- 451 3. Bhatt SP, Dransfield MT. Chronic obstructive pulmonary disease and cardiovascular
452 disease. *Transl Res* 2013;**162**:237–251.
- 453 4. Barr RG, Bluemke DA, Ahmed FS, Carr JJ, Enright PL, Hoffman EA, Jiang R, Kawut
454 SM, Kronmal RA, Lima JAC, Shahar E, Smith LJ, Watson KE. Percent emphysema,
455 airflow obstruction, and impaired left ventricular filling. *N Engl J Med* 2010;**362**:217–227.
- 456 5. Eckhardt CM, Balte PP, Barr RG, Bertoni AG, Bhatt SP, Cuttica M, Cassano PA, Chaves
457 P, Couper D, Jacobs DR, Kalhan R, Kronmal R, Lange L, Loehr L, London SJ, O’Connor
458 GT, Rosamond W, Sanders J, Schwartz JE, Shah A, Shah SJ, Smith L, White W, Yende S,
459 Oelsner EC. Lung function impairment and risk of incident heart failure: the NHLBI
460 Pooled Cohorts Study. *Eur Heart J* 2022;**43**:2196–2208.
- 461 6. Jörgensen K, Müller MF, Nel J, Upton RN, Houltz E, Ricksten SE. Reduced intrathoracic
462 blood volume and left and right ventricular dimensions in patients with severe
463 emphysema: An MRI study. *Chest* 2007;**131**:1050–1057.
- 464 7. Criner GJ, Connett JE, Aaron SD, Albert RK, Bailey WC, Casaburi R, Cooper JAD,
465 Curtis JL, Dransfield MT, Han MK, Make B, Marchetti N, Martinez FJ, Niewoehner DE,
466 Scanlon PD, Sciurba FC, Scharf SM, Sin DD, Voelker H, Washko GR, Woodruff PG,
467 Lazarus SC. Simvastatin for the prevention of exacerbations in moderate-to-severe COPD.
468 *N Engl J Med* 2014;**370**:2201–2210.
- 469 8. Vanfleteren LEGW, Spruit MA, Wouters EFM, Franssen FME. Management of chronic
470 obstructive pulmonary disease beyond the lungs. *Lancet Respir Med* 2016;**4**:911–924.
- 471 9. Paulus WJ, Tschöpe C. A novel paradigm for heart failure with preserved ejection

- 472 fraction: Comorbidities drive myocardial dysfunction and remodeling through coronary
473 microvascular endothelial inflammation. *J Am Coll Cardiol* 2013;**62**:263–271.
- 474 10. McDonagh TA, Metra M, Adamo M, Gardner RS, Baumbach A, Böhm M, Burri H,
475 Butler J, Celutkiene J, Chioncel O, Cleland JGF, Coats AJS, Crespo-Leiro MG, Farmakis
476 D, Gilard M, Heymans S. 2021 ESC Guidelines for the diagnosis and treatment of acute
477 and chronic heart failure. *Eur Heart J* 2021;**42**:3599–3726.
- 478 11. Heidenreich PA, Bozkurt B, Aguilar D, Allen LA, Byun JJ, Colvin MM, Deswal A,
479 Drazner MH, Dunlay SM, Evers LR, Fang JC, Fedson SE, Fonarow GC, Hayek SS,
480 Hernandez AF, Khazanie P, Kittleson MM, Lee CS, Link MS, Milano CA, Nnacheta LC,
481 Sandhu AT, Stevenson LW, Vardeny O, Vest AR, Yancy CW. 2022 AHA/ACC/HFSA
482 Guideline for the Management of Heart Failure. *J Am Coll Cardiol* 2022.
- 483 12. Jörgensen K, Houltz E, Westfelt U, Nilsson F, Scherstén H, Ricksten SE. Effects of Lung
484 Volume Reduction Surgery on Left Ventricular Diastolic Filling and Dimensions in
485 Patients with Severe Emphysema. *Chest* 2003;**124**:1863–1870.
- 486 13. Hohlfeld JM, Vogel-Claussen J, Biller H, Berliner D, Berschneider K, Tillmann H-C, Hittl
487 S, Bauersachs J, Welte T. Effect of lung deflation with indacaterol plus glycopyrronium
488 on ventricular filling in patients with hyperinflation and COPD (CLAIM): a double-blind,
489 randomised, crossover, placebo-controlled, single-centre trial. *Lancet Respir Med*
490 2018;**6**:368–378.
- 491 14. Rabe KF, Hurst JR, Suissa S. Cardiovascular disease and COPD: dangerous liaisons? *Eur*
492 *Respir Rev* 2018;**27**:180057.
- 493 15. Oudijk EJD, Lammers JWJ, Koenderman L. Systemic inflammation in chronic obstructive
494 pulmonary disease. *Eur Respir J* 2003;**22**:5s-13s.

- 495 16. Buczek-Thomas JA, Lucey EC, Stone PJ, Chu CL, Rich CB, Carreras I, Goldstein RH,
496 Foster JA, Nugent MA. Elastase Mediates the Release of Growth Factors from Lung In
497 Vivo. *Am J Respir Cell Mol Biol* 2004;**31**:344–350.
- 498 17. Petta A Di, Simas R, Ferreira CL, Capelozzi VL, Salemi VMC, Moreira LFP, Sannomiya
499 P. Effects of the association of diabetes and pulmonary emphysema on cardiac structure
500 and function in rats. *Int J Exp Pathol* 2015;**96**:350–357.
- 501 18. Sato S, Kato S, Arisaka Y, Takahashi H, Tomoike H. Pulmonary haemodynamics in
502 awake rats following treatment with endotracheal pancreatic elastase. *Eur Respir J*
503 1994;**7**:1294–1299.
- 504 19. Padilha G de A, Horta LFB, Moraes L, Braga CL, Oliveira M V., Santos CL, Ramos IP,
505 Morales MM, Capelozzi VL, Goldenberg RCS, Abreu MG de, Pelosi P, Silva PL, Rocco
506 PRM. Comparison between effects of pressure support and pressure-controlled ventilation
507 on lung and diaphragmatic damage in experimental emphysema. *Intensive Care Med Exp*
508 2016;**4**:35.
- 509 20. Ceelen JJM, Schols AMWJ, Kneppers AEM, Rosenbrand RPHA, Drozd MM, Hoof SJ
510 Van, Theije CC De, Kelders MCJM, Verhaegen F, Langen RCJ. Altered protein turnover
511 signaling and myogenesis during impaired recovery of inflammation-induced muscle
512 atrophy in emphysematous mice. *Sci Rep* 2018;**8**:1–12.
- 513 21. Oliveira MV De, Novaes Rocha N De, Santos RS, Macedo Rocco MR, Magalhães RF De,
514 Silva JD, Lopes Souza SA, Capelozzi VL, Pelosi P, Leme Silva P, Macedo Rocco PR.
515 Endotoxin-induced emphysema exacerbation: A novel model of chronic obstructive
516 pulmonary disease exacerbations causing cardiopulmonary impairment and diaphragm
517 dysfunction. *Front Physiol* 2019;**10**.

- 518 22. Amancio G de CS, Grabe-Guimarães A, Haikel D, Moreau J, Barcellos NMS,
519 Lacampagne A, Matecki S, Cazorla O. Effect of pyridostigmine on in vivo and in vitro
520 respiratory muscle of mdx mice. *Respir Physiol Neurobiol* 2017;**243**:107–114.
- 521 23. Chakouri N, Reboul C, Boulghobra D, Kleindienst A, Nottin S, Gayraud S, Roubille F,
522 Matecki S, Lacampagne A, Cazorla O. Stress-induced protein S-glutathionylation and
523 phosphorylation crosstalk in cardiac sarcomeric proteins - Impact on heart function. *Int J*
524 *Cardiol* 2018;**258**:207–216.
- 525 24. Andre L, Boissière J, Reboul C, Perrier R, Zalvidea S, Meyer G, Thireau J, Tanguy S,
526 Bideaux P, Hayot M, Boucher F, Obert P, Cazorla O, Richard S. Carbon monoxide
527 pollution promotes cardiac remodeling and ventricular arrhythmia in healthy rats. *Am J*
528 *Respir Crit Care Med* 2010;**181**:587–595.
- 529 25. Thurlbeck WM. Internal surface area and other measurements in emphysema. *Thorax*
530 1967;**22**:483–496.
- 531 26. Andre L, Fauconnier J, Reboul C, Feillet-Coudray C, Meschin P, Farah C, Fouret G,
532 Richard S, Lacampagne A, Cazorla O. Subendocardial increase in reactive oxygen species
533 production affects regional contractile function in ischemic heart failure. *Antioxidants*
534 *Redox Signal* 2013;**18**:1009–1020.
- 535 27. Cazorla O, Szilagyi S, Guennec J Le, Vassort G, Lacampagne A. Transmural
536 stretch-dependent regulation of contractile properties in rat heart and its alteration after
537 myocardial infarction. *FASEB J* 2005;**19**:88–90.
- 538 28. Roh J, Hill JA, Singh A, Valero-Muñoz M, Sam F. Heart Failure With Preserved Ejection
539 Fraction: Heterogeneous Syndrome, Diverse Preclinical Models. *Circ Res*
540 2022;**130**:1906–1925.

- 541 29. Ceelen JJM, Schols AMWJ, Hoof SJ van, Theije CC de, Verhaegen F, Langen RCJ.
542 Differential regulation of muscle protein turnover in response to emphysema and acute
543 pulmonary inflammation. *Respir Res* 2017;**18**:75.
- 544 30. Fonseca LMC da, Reboredo MM, Lucinda LMF, Fazza TF, Rabelo MAE, Fonseca AS,
545 Paoli F de, Pinheiro BV. Emphysema induced by elastase enhances acute inflammatory
546 pulmonary response to intraperitoneal LPS in rats. *Int J Exp Pathol* 2016;**97**:430–437.
- 547 31. Kobayashi S, Fujinawa R, Ota F, Kobayashi S, Angata T, Ueno M, Maeno T, Kitazume S,
548 Yoshida K, Ishii T, Gao C, Ohtsubo K, Yamaguchi Y, Betsuyaku T, Kida K, Taniguchi N.
549 A single dose of lipopolysaccharide into mice with emphysema mimics human Chronic
550 obstructive pulmonary disease exacerbation as assessed by micro-computed tomography.
551 *Am J Respir Cell Mol Biol* 2013;**49**:971–977.
- 552 32. Oliveira M V., Abreu SC, Padilha GA, Rocha NN, Maia LA, Takiya CM, Xisto DG, Suki
553 B, Silva PL, Rocco PRM. Characterization of a mouse model of emphysema induced by
554 multiple instillations of low-dose elastase. *Front Physiol* 2016;**7**:1–12.
- 555 33. Henriques I, Padilha GA, Huhle R, Wierzchon C, Miranda PJ, Ramos IP, Rocha N, Cruz
556 FF, Santos RS, Oliveira M V de, Souza SA, Goldenberg RC, Luiz R, Pelosi P, Gama de
557 Abreu M, Silva PL, Rocco PR. Comparison between variable and conventional volume-
558 controlled ventilation on cardiorespiratory parameters in experimental emphysema. *Front*
559 *Physiol* 2016;**7**:277.
- 560 34. Smith BM, Prince MR, Hoffman EA, Bluemke DA, Liu CY, Rabinowitz D, Hueper K,
561 Parikh MA, Gomes AS, Michos ED, Lima JAC, Barr RG. Impaired left ventricular filling
562 in COPD and emphysema: Is it the heart or the lungs?: The multi-ethnic study of
563 atherosclerosis COPD study. *Chest* 2013;**144**:1143–1151.

- 564 35. Lüthje L, Raupach T, Michels H, Unsöld B, Hasenfuss G, Kögler H, Andreas S. Exercise
565 intolerance and systemic manifestations of pulmonary emphysema in a mouse model.
566 *Respir Res* 2009;**10**.
- 567 36. Hegemann N, Primessnig U, Bode D, Wakula P, Beindorff N, Klopfleisch R, Michalick L,
568 Grune J, Hohendanner F, Messroghli D, Pieske B, Kuebler WM, Heinzl FR. Right-
569 ventricular dysfunction in HFpEF is linked to altered cardiomyocyte Ca²⁺ homeostasis
570 and myofilament sensitivity. *ESC Hear Fail* 2021;**8**:3130–3144.
- 571 37. SOLARO RJ, MOIR AJG, PERRY S V. Phosphorylation of troponin I and the inotropic
572 effect of adrenaline in the perfused rabbit heart. *Nature* 1976;**262**:615–617.
- 573 38. Biesiadecki BJ, Kobayashi T, Walker JS, Solaro RJ, Tombe PP De. The troponin C
574 G159D mutation blunts myofilament desensitization induced by troponin I Ser23/24
575 phosphorylation. *Circ Res* 2007;**100**:1486–1493.
- 576 39. Dhot J, Ferron M, Prat V, Persello A, Roul D, Stévant D, Guijarro D, Piriou N, Aillerie V,
577 Erraud A, Toumaniantz G, Erfanian M, Tesse A, Grabherr A, Tesson L, Menoret S,
578 Anegon I, Trochu JN, Steenman M, Waard M De, Rozec B, Lauzier B, Gauthier C.
579 Overexpression of endothelial β ₃-adrenergic receptor induces diastolic dysfunction in rats.
580 *ESC Hear Fail* 2020;**7**:4159–4171.
- 581 40. Lund LH, Benson L, Dahlström U, Edner M, Friberg L. Association between use of β -
582 blockers and outcomes in patients with heart failure and preserved ejection fraction. *JAMA*
583 - *J Am Med Assoc* 2014;**312**:2008–2018.
- 584 41. Hernandez AF, Hammill BG, O'Connor CM, Schulman KA, Curtis LH, Fonarow GC.
585 Clinical Effectiveness of Beta-Blockers in Heart Failure. *J Am Coll Cardiol* 2009;**53**:184–
586 192.

- 587 42. Flather MD, Shibata MC, Coats AJS, Veldhuisen DJ Van, Parkhomenko A, Borbola J,
588 Cohen-Solal A, Dumitrascu D, Ferrari R, Lechat P, Soler-Soler J, Tavazzi L, Spinarova L,
589 Toman J, Böhm M, Anker SD, Thompson SG, Poole-Wilson PA. FASTTRACK
590 Randomized trial to determine the effect of nebivolol on mortality and cardiovascular
591 hospital admission in elderly patients with heart failure (SENIORS). *Eur Heart J*
592 2005;**26**:215–225.
- 593 43. Conraads VM, Metra M, Kamp O, Keulenaer GW De, Pieske B, Zamorano J, Vardas PE,
594 Böhm M, Dei Cas L. Effects of the long-term administration of nebivolol on the clinical
595 symptoms, exercise capacity, and left ventricular function of patients with diastolic
596 dysfunction: Results of the ELANDD study. *Eur J Heart Fail* 2012;**14**:219–225.
- 597 44. Dransfield MT, Voelker H, Bhatt SP, Brenner K, Casaburi R, Come CE, Cooper JAD,
598 Criner GJ, Curtis JL, Han MK, Hatipoğlu U, Helgeson ES, Jain V V, Kalhan R, Kaminsky
599 D, Kaner R, Kunisaki KM, Lambert AA, Lammi MR, Lindberg S, Make BJ, Martinez FJ,
600 McEvoy C, Panos RJ, Reed RM, Scanlon PD, Sciruba FC, Smith A, Sriram PS, Stringer
601 WW, Weingarten JA, Wells JM, Westfall E, Lazarus SC, Connett JE. Metoprolol for the
602 Prevention of Acute Exacerbations of COPD. *N Engl J Med* 2019;**381**:2304–2314.
- 603 45. MacNee W. Beta-Blockers in COPD — A Controversy Resolved? *N Engl J Med*
604 2019;**381**:2367–2368.
- 605 46. Moulin M, Piquereau J, Mateo P, Fortin D, Rucker-Martin C, Gressette M, Lefebvre F,
606 Gresikova M, Solgadi A, Veksler V, Garnier A, Ventura-Clapier R. Sexual Dimorphism
607 of Doxorubicin-Mediated Cardiotoxicity. *Circ Hear Fail* 2015;**8**:98–108.
- 608 47. Ino T, Aviado DM. Cardiopulmonary effects of progestational agents in emphysematous
609 rats. *Chest* 1971;**59**:659–666.

- 610 48. Stolz D, Mkorombindo T, Schumann DM, Agusti A, Ash SY, Bafadhel M, Bai C,
611 Chalmers JD, Criner GJ, Dharmage SC, Franssen FME, Frey U, Han M, Hansel NN,
612 Hawkins NM, Kalhan R, Konigshoff M, Ko FW, Parekh TM, Powell P, Rutten-van
613 Mölken M, Simpson J, Sin DD, Song Y, Suki B, Troosters T, Washko GR, Welte T,
614 Dransfield MT. Towards the elimination of chronic obstructive pulmonary disease: a
615 Lancet Commission. *Lancet* 2022;**400**:921–972.
- 616 49. Wright JL, Cosio M, Churg A. Animal models of chronic obstructive pulmonary disease.
617 *Am J Physiol Cell Mol Physiol* 2008;**295**:L1–L15.
- 618 50. Churg A, Sin DD, Wright JL. Everything Prevents Emphysema. *Am J Respir Cell Mol*
619 *Biol* 2011;**45**:1111–1115.

620

621

622 **Figure legends:**

623

624 **Figure 1:** Chronic emphysema rat model with exacerbation.

625 (A) Illustration of the protocol and treatment procedures. (B) Lung sections at X10 of control (Ctrl)
626 and ELA-LPS animals stained with hematoxylin-eosin. Mean linear intercept (n=13 control and 6
627 ELA-LPS animals, 4 cuts, 6 areas per cut) (scale bar=100µm). (C-D) *In-vivo* exploration of
628 pulmonary function using whole body plethysmography analysis of (C) peak inspiratory flow (D)
629 and peak expiratory flow (n=13 control and 10 ELA-LPS animals). (E-F) Maximal incremental
630 metabolic exercise test exploration with (E) VO₂max and (F) maximum running distance (n=9
631 animals per group). Differences were assessed by Student t-test *p<0.05.

632

633 **Figure 2:** Echocardiography indicates HFpEF in ELA-LPS rats.

634 *In-vivo* contractile function assessed by echocardiography with (A) left ventricular ejection
635 fraction assessed by M-mode long axis, (B) E/A ratio by mitral flow power Doppler, and (C) E/e'
636 ratio by mitral tissue Doppler. Data are presented as mean ± SEM; n =22 controls and 19 ELA-
637 LPS animals. Differences were assessed by Mann-Whitney test *p<0.05.

638

639 **Figure 3:** Myocardial hypertrophy without fibrosis in ELA-LPS rats.

640 (A) The collagen content was explored in 6µm cardiac tissue sections stained with picrosirius red
641 to reveal collagen of myocardial (left) or perivascular tissues (right); n=5 Ctrl and 4 ELA-LPS
642 animals, 4 slides per animal, 3 areas per slide in the free wall are illustrated by black rectangles.
643 (B) Heart weight to body weight ratio; n=44 Ctrl and 18 ELA-LPS animals. (C) Membrane intact
644 isolated left ventricular myocytes cell surface area; n=20 cells *per* animal, 5 animals *per* group.

645 (A) and (C) are represented as median with total distribution and 25 – 50% interquartile. (B) is
646 represented as mean \pm SEM. Differences were assessed by Mann-Whitney test $*p<0.05$.

647

648 **Figure 4:** *Ex-vivo* altered myocardial cellular function.

649 Isolated left ventricular myocyte functional tests were performed with an IonOptix cell system
650 under unattached conditions. Representative recordings of Control (Ctrl) and ELA-LPS myocytes
651 are shown in the left panels. (A-D) Intracellular Ca^{2+} parameters indexed by indo-1 fluorescence:
652 (B) basal diastolic calcium level and (C) Ca^{2+} transient amplitude (both expressed in 405/480 nm
653 ratiometric units), as well as (D) the Ca^{2+} reuptake time constant “tau”. (E-H) Contractile
654 properties as indexed by (F) basal sarcomere length (SL), (G) SL shortening extent and (H) SL
655 relaxation velocity. n= 11 Ctrl and 9 ELA-LPS animals, 36-45 cells per animal. (B), (C), (D), (F),
656 (G) and (H) are represented as median with total distribution and 25 – 50% interquartile.
657 Differences were assessed by Mann-Whitney test $*p<0.05$.

658

659 **Figure 5:** *Ex-vivo* altered cardiac myofilament function.

660 Myofilament function was assessed in left ventricular permeabilized cardiomyocytes that were
661 attached to a force transducer and stretched to 2.3 μ m sarcomere length; cells were activated over
662 a range of $[Ca^{2+}]$. (A) Average normalized maximal tension – pCa relationships (mean \pm SEM).
663 Myofilament contractile function indices were measured: (B) maximal normalized tension, (C)
664 myofilament Ca^{2+} sensitivity (pCa_{50}) and (E) myofilament cross-bridge cycling rate, as indexed
665 by the K_{tr} parameter, which is obtained from a rapid release-restretch maneuver as illustrated in
666 the top panel (D). n=5 Ctrl and 6 ELA-LPS animals with 8 cells per animal. (B), (C) and (E) are

667 represented as median with total distribution and 25 – 50% interquartile. Differences were
668 assessed by Mann-Whitney test $*p < 0.05$.

669

670 **Figure 6:** Increased β -adrenergic level and improvement of HFpEF following β -blocker
671 treatment.

672 (A) The impact of adrenergic stimulation following dobutamine injection was assessed by the
673 increase in heart rate measured by telemetric ECG (Δ HR= difference of heart rate after and
674 before dobutamine injection); n = 17 Ctrl, 10 ELA-LPS animals, and 9 ELA-LPS+ β^- groups. (B)
675 Representative Western-Blots of Troponin-I (TnI) Serine²²⁻²³ PKA mediated phosphorylation
676 (down panel) and quantification (top panel) in the control, ELA-LPS and ELA-LPS+ β^- groups;
677 phosphorylation was normalized to total TnI content; n=10 Ctrl, 10 ELA-LPS and 6 ELA-
678 LPS+ β^- animals, 2-4 replicates per blot. The *in-vivo* impact of 5-week Bisoprolol treatment (n= 9
679 animals) was assessed by (C) mitral E/e' ratio from tissue Doppler, (D) left ventricular ejection
680 fraction. Compared with n = 19 and 9 ELA-LPS animals for echocardiography and ECG
681 respectively and 9 ELA-LPS+ β^- groups. Analysis of differences for panel (B) and (D) was
682 assessed by one-way ANOVA analysis followed by Bonferroni's multiple-comparisons test.
683 Data are represented as mean \pm SEM. Differences for panel (A), (C) were assessed by Kruskal-
684 Wallis test with Dunn's correction for the multiple comparison post hoc test. $*p < 0.05$.

685

686 **Figure 7:** Improvement of cellular cardiomyopathy following β -blocker treatment.

687 Animals were treated 1 day post ELA-LPS installation for 5-weeks with Bisoprolol (in the drinking
688 water). (A-D) Membrane intact unloaded isolated myocytes excitation-contraction parameters
689 assessed with the IonOptix cell system included (A) basal sarcomere length, (B) basal diastolic

690 $[Ca^{2+}]$, (C) Ca^{2+} transient amplitude, and (D) the Ca^{2+} reuptake time constant “tau”; n= 11 Ctrl, 9
691 ELA-LPS and 5 β 1-blocker treated animals, 36-45 cells per animal. (E-G) Myofilament properties
692 as assessed in mechanically loaded permeabilized isolated myocyte (SL=2.3 mm) included (E)
693 maximal normalized tension (Tmax), (F) myofilament Ca^{2+} sensitivity (pCa_{50}), and (G) cross-
694 bridge cycling rate (K_{tr}); n=5 Ctrl, 6 ELA-LPS and 4 β 1-blocker treated animals, 7-8 cells per
695 animal. A-G are represented as median with total distribution and 25 – 50% interquartile.
696 Differences for panel (A), (B), (C), (D) and (E) were assessed by Kruskal-Wallis test with Dunn’s
697 correction for the multiple comparison post hoc test. (F) and (G) differences were assessed by one-
698 way ANOVA analysis followed by Bonferroni’s multiple-comparisons test. P-value were
699 significant <0.05 , * difference compared to Ctrl group, \$ difference compared to ELA-LPS
700 group.

701

702 **Graphical abstract:** The present work is a preliminary study of a COPD- exacerbated emphysema
703 cardiac outcomes animal model. It highlights the implication of β -adrenergic stimulation inducing
704 a heart failure with preserved ejection fraction pattern (HFpEF) that involve cardiomyocytes
705 sarcomere alterations and appears to be reversed by β 1-blocker therapy.

706

Figure 1

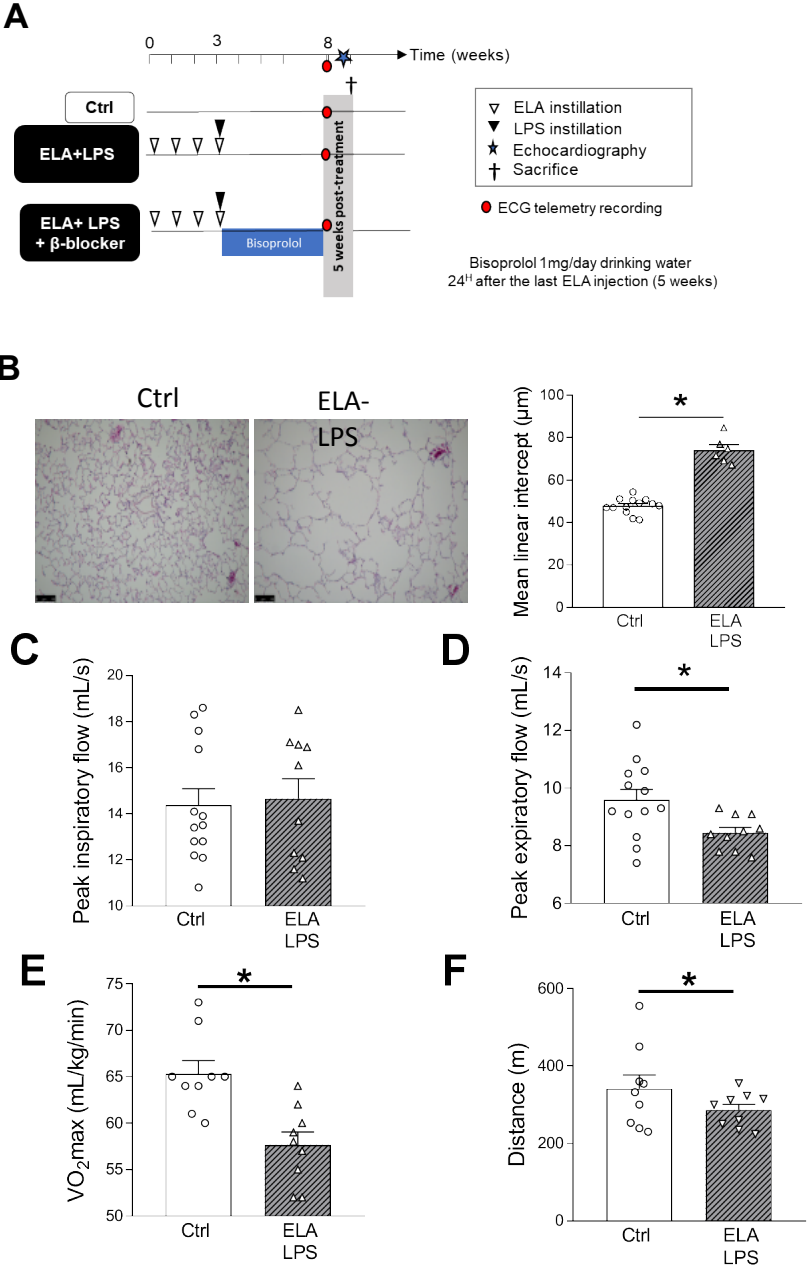


Figure 2

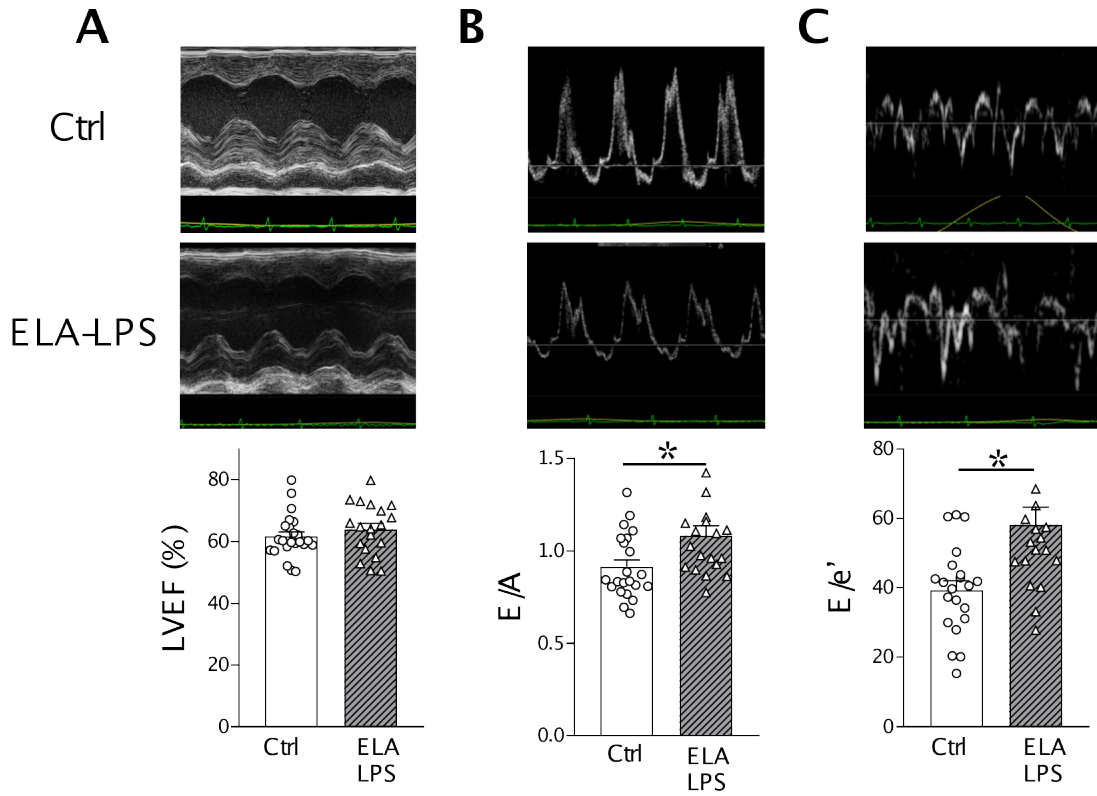


Figure 3

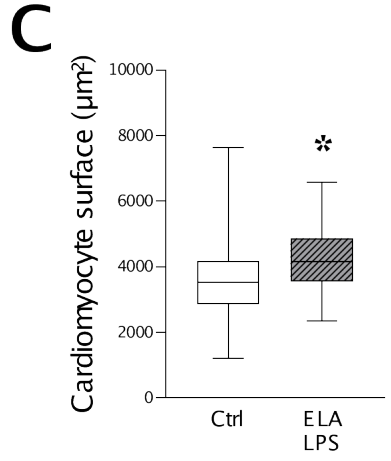
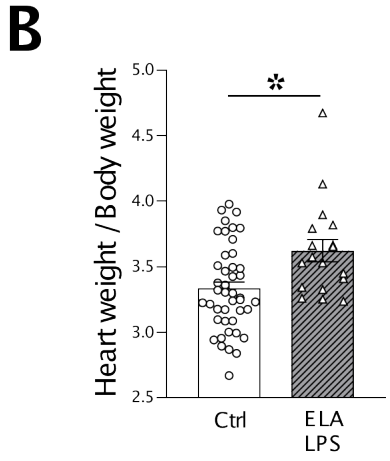
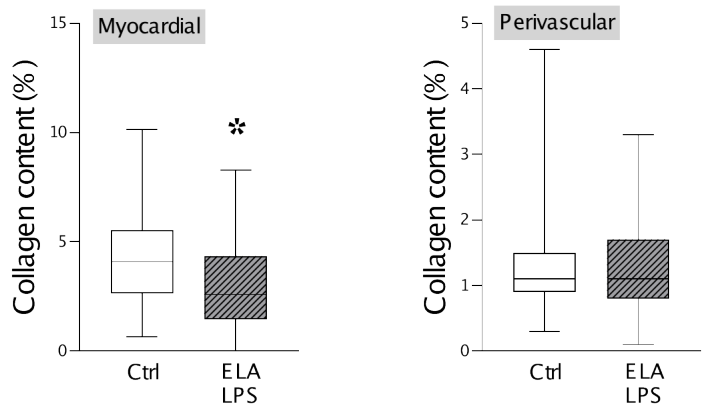
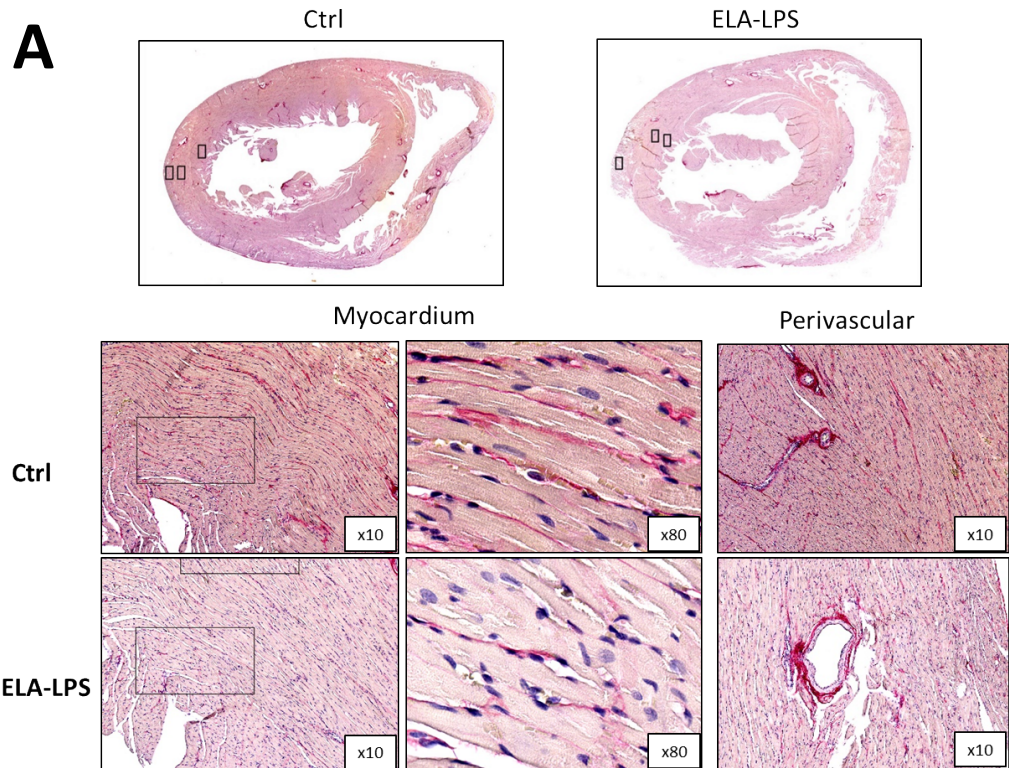


Figure 4

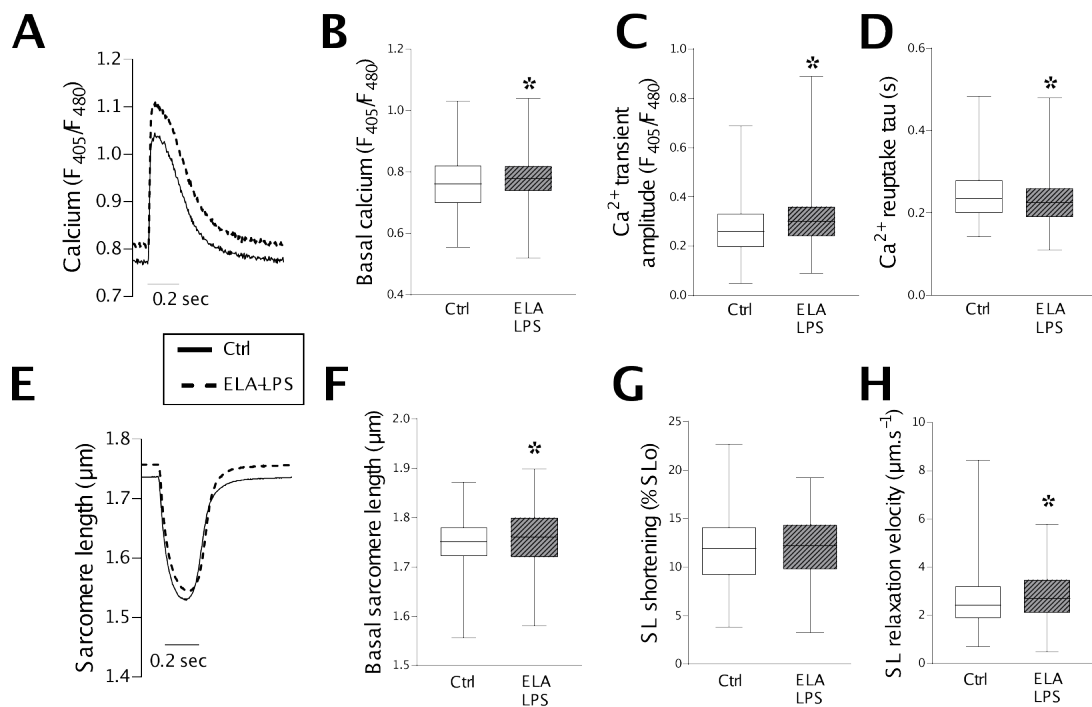


Figure 5

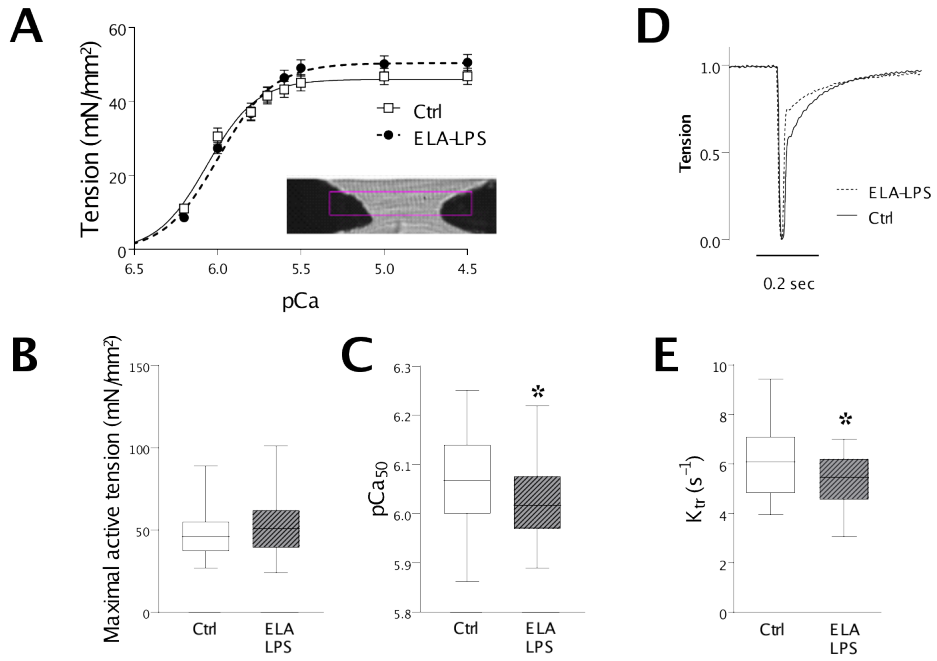


Figure 6

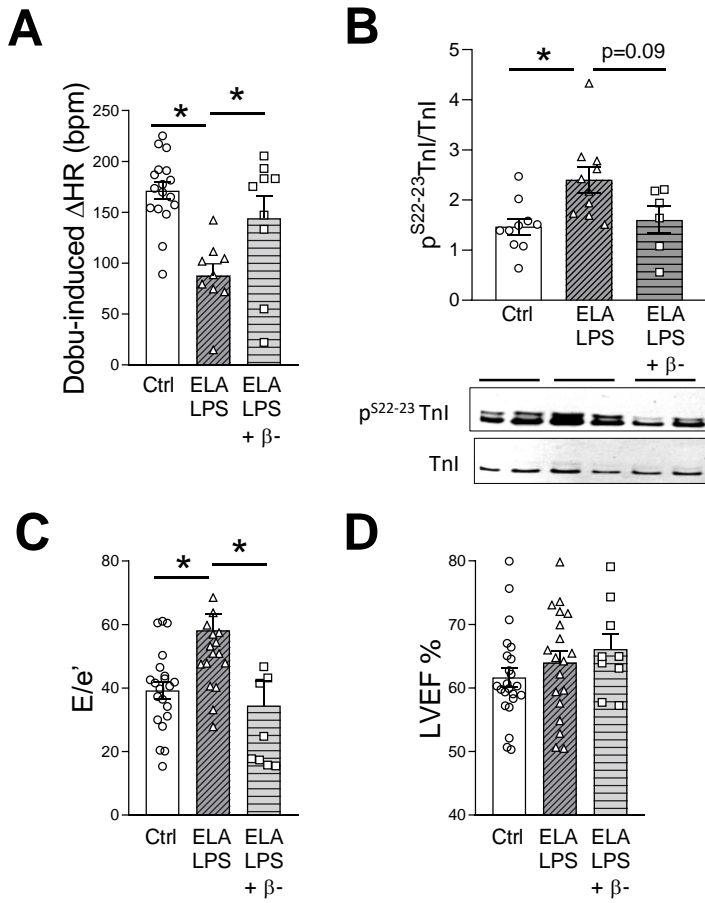
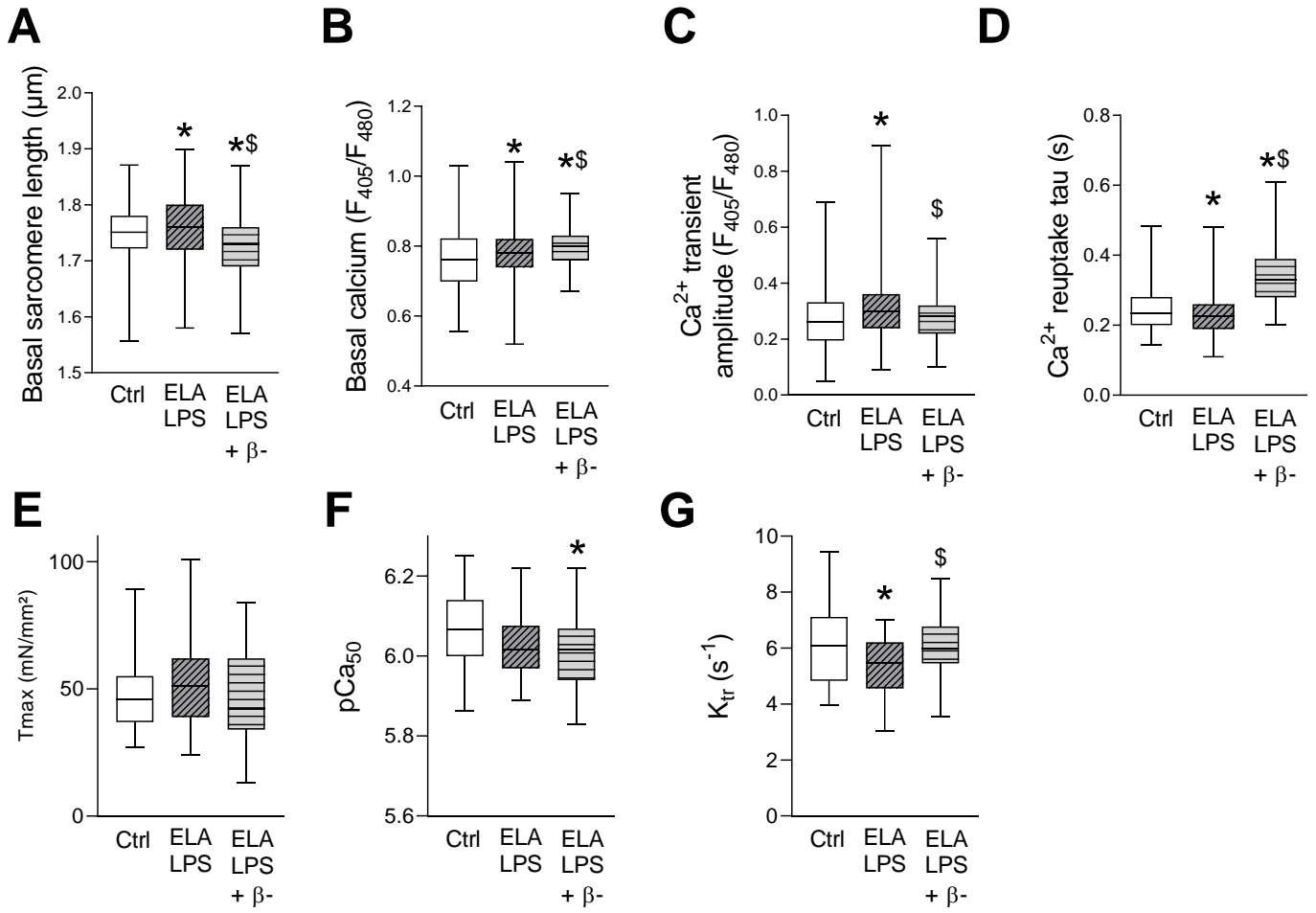


Figure 7



Supplemental data

1
2
3
4
5
6
7
8
9
10
11
12
13
14
15
16
17
18
19

Diastolic cardiomyopathy secondary to experimentally induced exacerbated emphysema

Pierre-Edouard Grillet, Elodie Desplanche, Quentin Wynands, Fares Gouzi, Patrice Bideaux, Aurelie Fort, Valérie Scheuermann, Alain Lacampagne, Anne Virsolvy, Jérôme Thireau, Pieter de Tombe, Arnaud Bourdin*, Olivier Cazorla*

*Equal contribution

Phymedexp INSERM, CNRS, Université de Montpellier, CHRU Montpellier, France.

Correspondence to:

Olivier CAZORLA

PhyMedExp, Université de Montpellier, INSERM, CNRS,

CHU Arnaud de Villeneuve

34295 Montpellier, France

Phone: +33 467 41 52 44

Fax: +33 467 41 52 42

olivier.cazorla@inserm.fr

21 **Materials**

22

23

24 **Elastase-induced emphysema rat model**

25 All investigations conformed to European Parliament Directive 2010/63/EU and were
26 approved by the local ethics committee rules “Comité d'éthique pour l'expérimentation
27 animale Languedoc-Roussillon” (APAFIS#13133-2018012212031585v2).

28

29 Under gaseous anesthesia Isoflurane (2.5%/O₂), emphysema was induced in seven weeks old
30 male rat (Janvier Labs, France) by oro-tracheal instillation of pancreatic porcine elastase (ELA,
31 4 units/200µL saline solution, Sigma-Aldrich, France) once a week for four weeks. To mimic
32 COPD exacerbations, animals received with last ELA installation, lipopolysaccharide (LPS, E.
33 coli O55:B5, 2.5mg/kg, Sigma-Aldrich, France). Animals treated the same way without
34 receiving instillations served as controls (Ctrl) (Figure 1A). As a regulatory requirement, one
35 buprenorphine injection (0.05 mg/kg) was given to avoid pain just after instillation. Animals
36 were investigated 5 weeks after last instillation. One group of ELA-LPS animals received
37 bisoprolol, a β ₁ receptor-specific blocker (2.5mg/kg/day in drinking water, bisoprolol
38 hemifumarate, MedChemExpress, USA) from day 1 after the last ELA-LPS instillation until
39 sacrifice.

40

41 **Histological characterization of emphysema, fibrosis and inflammation**

42 At the end of the protocol, the lungs and heart were rapidly harvested after anesthesia (140
43 mg/kg sodium pentobarbital, *i.p.*) and total loss of consciousness. The lungs were inflated to

44 25cm H₂O with 4% formol *via* cannulation through the trachea and then immersed in 4%
45 formol for histology analysis. The heart was directly immersed in 4% formol. Lungs lobes were
46 separated after formol fixation. Organs were properly rinsed, dehydrated in progressive
47 ethanol baths, and embedded in paraffin. Six micrometers thick lung tissue sections apposed
48 on slides were then stained with hematoxylin and eosin to assess the alveolar morphology
49 organization. Emphysema was characterized using mean linear intercept (Lm) method with an
50 Olympus microscope, 5X magnification. Briefly, using CellP program (Olympus), a grid was
51 applied on the field with a 50µm spacing between lines. The software automatically detects
52 the intercepts between the grid and alveoli, then the number of intercepts was divided by the
53 total length¹.

54 Automated red picosirius staining was performed on 6µm cardiac tissue sections (Bio Optica
55 red picosirius picrate, Italy) at the histologic platform of the Department of Pathology of the
56 Montpellier University Hospital. Stained slides were scanned with a slide scanner
57 (Nanozoomer, Hamamatsu, Japan). Analysis of myocardial and perivascular tissue content in
58 collagen was performed using ImageJ software (Image J, USA) and fibrosis area was measured
59 automatically with the MRI Fibrosis Tool
60 (https://github.com/MontpellierRessourcesImagerie/imagej_macros_and_scripts/wiki/MRI_Fibrosis_Tool,
61 last access on 20 April 2022). The person who performed the automatic analysis
62 was blinded on the identity of the images. For each heart, we obtained 12 data points. We
63 analyzed 2 different sections from the basal part of the heart and 2 different sections for the
64 apical part. In each section of the heart we analyzed 3 regions in the freewall corresponding
65 of the sub-epicardium/mid-wall and sub-endocardium. Eight perivascular sections per slide
66 were randomly selected to measure percentage of red coloration over total area section. The

67 areas that did not contain any tissue (inside the vessels or damages parts of the section) were
68 excluded from the total area using the same modified tool.

69 After deparaffinization and rehydration, tissue slides were subjected to antigen retrieval by
70 pepsin. Lung sections were stained for neutrophils and eosinophils with vectastain kit (vector
71 laboratories). Briefly, after peroxidase and alkaline phosphatase activity blocking with bloxall
72 (vector laboratories), sections were blocked with 10% normal horse serum 10 min following
73 by 1 hour incubation with a mouse anti human eosinophil major basic protein antibody
74 (Biorad), or a rabbit anti human neutrophil elastase antibody (abcam). After rinsing a
75 biotinylated secondary anti mouse rat adsorbed IgG antibody (vector laboratories) or
76 biotinylated anti rabbit IgG antibody (vector laboratories) was added for 30 minutes, followed
77 by the addition of a peroxidase/streptavidin complex (VECTASTAIN universal kit; Vector
78 Laboratories, Peterborough, United Kingdom). Diaminobenzidine (vector laboratories) was
79 used to visualize the antigen of interest. Sections were counterstained using hematoxylin.
80 Stained slides were scanned with a slide scanner (Nanozoomer, Hamamatsu, Japan).
81 Quantification of the number of neutrophils and eosinophils was performed by cumulative
82 counts on 5 fields of bronchiole or alveola or vessel view per section. For bronchiole,
83 neutrophil and eosinophil number was expressed in number/ μm of perimeter of bronchiole.
84 For alveola, one field is a square of 0.407mm^2 and neutrophil and eosinophil were expressed
85 as number/ mm^2 . For vessels, they were expressed in number/ μm of perimeter of internal
86 adventitia.

87

88 **Maximal oxygen consumption ($V'O_2$ max)**

89 The maximal oxygen consumption ($V'O_2$ max) is measured by an incremental exercise test
90 (EFX) performing on a metabolic treadmill coupled to a gas analyzer system (Oxymax,

91 Columbus Instruments, Columbus, USA). The implemented protocol was adapted from Musch
92 *et al*². A first habituation phase, lasting 5 days, was carried out in the animals, one week before
93 the test carried out³.

94 During the EFX the rat have a period of acclimation of 5 min at rest, then the treadmill protocol
95 starts with a speed of 10 m/min and gradual increase in speed in steps of 5m/min every 3
96 minutes until the animal is exhausted. Exhaustion was defined as the animal remaining on the
97 electrical stimulation grid without attempting to re-engage the treadmill within 15 seconds.

98 The $V'O_2$ and $V'CO_2$ flow rates are calculated based on the measurement of the fractions in O_2
99 (FO_2 , in %) and in CO_2 (FCO_2 , in %) at the inlet and at the outlet of a sealed chamber every 30
100 seconds (Oxymax, Columbus Instruments). $V'O_2$ max was defined as the higher value of $V'O_2$
101 obtained (average of 30 seconds) before stopping the effort.

102

103 **Western blot analysis**

104 PKA dependent myocardial protein phosphorylation was studied, as previously described⁴.
105 Briefly, frozen LV tissue powdered using tissue grinder on dry-ice and solubilized in non-
106 reducing Laemmli buffer. Proteins were separated using gradient SDS-PAGE electrophoresis
107 and transferred onto membranes (nitrocellulose, GE Healthcare, USA). Membranes were
108 blocked with the Odyssey Blocking Buffer in TBS (LI-COR Biosciences, USA) and incubated
109 overnight with primary antibodies. Bands were revealed and quantified with the Odyssey
110 system (LI-COR Biosciences, USA) after incubation with fluorescent secondary antibodies.
111 Phosphorylation level was expressed relative to total protein content, and protein content
112 was normalized to GAPDH content.

113

114 **Plasma multiplex cytokine analysis**

115 Six plasma cytokines (IL-1 β , IL-4, IL-6, IL-10, IL-13 and KC/GRO) were measured using
116 chemiluminescence-based assays from Meso Scale Discovery (MSD, Gaithersburg, MD, USA).
117 For the 6 cytokines, a V-PLEX Pro-Inflammatory Panel 2 Rat Kit was used (MSD, Gaithersburg,
118 MD, USA). The detection ranges are IL-1 β 6.92–8100 pg/mL, IL-4 0.69–723 pg/mL, IL-6 13.8–
119 8550 pg/mL, IL-10 16.4–15 700 pg/mL, IL-13 1.97–1080 pg/mL, and KC/GRO 1.04–728 pg/mL.
120 All assays were performed in duplicate. Analyses were done using a QuickPlex SQ 120
121 instrument (MSD, Gaithersburg, MD, USA) and DISCOVERY WORKBENCH[®] 4.0 software. All
122 samples were run at the same time.

123

124 ***In vivo* respiratory function**

125 Respiratory function was analyzed the day before sacrifice using a whole-body
126 plethysmograph (Emka Technologies, France) and the Iox2 software (Emka Technologies,
127 France) as previously described⁵. Animals were first familiarized with the chamber the week
128 before the test. After 30 min stabilization, each animal was visually monitored and ventilatory
129 parameters were recorded during inactive phase for 15 min under two experimental
130 conditions. Animals were exposed to room air (1.5L/min inflow). The parameters measured
131 were inspiration time (Ti), expiration time (Te), minute-volume (MV), tidal-volume (TV), peak
132 inspiratory flow (PIF), peak expiratory flow (PEF), expiratory flow 50 (EF50), relaxation time
133 (RT), frequency of breathing (f), enhanced pause (PenH) and EV (expired volume).

134

135 ***In vivo* cardiac function by echocardiography and ECG telemetry**

136 *In vivo* contractile cardiac function was explored using an echocardiograph (Vevo 3100,
137 Visualsonics, Canada) with a 20 MHz probe as previously⁶. Animals were anesthetized with
138 Isoflurane (2.5 – 3.5%) under 1L/min air. Particular attention has been paid to ensure that the

139 heart rate was the same in all groups to allow proper comparison of the echocardiography
140 data, in bpm: ctrl (358 ± 4.9), ELA-LPS (355 ± 6.0), and ELA-LPS+ β -blocker (357 ± 14.9).
141 Following ESC working group position paper ⁷, long axis B and M-mode were acquired in
142 parasternal long axis. Short axis B, M-mode, 4 cavity chamber view, Doppler and tissular
143 Doppler were acquired in parasternal short axis. Aortic and pulmonary artery view were
144 acquired in modified parasternal short axis.

145 For electrocardiogram (ECG) recordings, rats were equipped with telemetric transmitter (CA-
146 F40, Data Sciences International, St. Paul, MN, U.S.A) under general anesthesia (Isoflurane,
147 2.5% in O₂) and allowed to recover for 15 days⁸. Rats were monitored with ECG recordings by
148 using a signal RCP-1 receiver connected to a data acquisition system (Ponemah Physiology
149 Platform v6.42, DSI). The basal ECG *i.e.* without forced-exercise were collected continuously
150 over 24 h at a sampling rate of 2 kHz in a calm and quiet room. Successive RR interval series
151 were obtained using Ponemah Physiology Platform from 8 hours ECG recording, taking in the
152 same time slot for all animals (10:00 PM to 06:00 AM). PR, QRS and QT intervals were
153 determined from the same ECG segment.

154 For pharmacological testing with dobutamine (2mg/kg, *i.p.*), ECG was recorded 4 hours before
155 and 4 hours after the injection. Each dobutamine challenge was continuously followed
156 through automatic RR detection, from which the data describing the most profound changes
157 were chosen for the analysis of cardiac reserve. These changes were selected from the most
158 significant decrease in RR intervals and results (mean over at least 8 000 cardiac cycle PQRST)
159 were compared between pre-dosing and post-dosing periods.

160

161 ***In vivo* non-invasive systemic pressure measurement**

162 Non-invasive systemic pressure was measured by a tail-cuff apparatus (Coda[®] High
163 throughput system, non-invasive pressure system, Kent Scientific, USA) under temperature-
164 controlled conditions (25°C). After a week of familiarization to the procedure, animals were
165 placed inside the system, and recorded during 15 minutes with maximal occlusion pressure of
166 250 mmHg. Five good quality recordings were used to mean the pressure.

167

168 **Cardiac excitation-contraction coupling**

169 Intact cardiomyocytes were isolated from the heart by enzymatic digestion as previously
170 described ⁹. Briefly, the heart was harvested while beating and quickly cannulated on a
171 Langendorff apparatus by the aorta. The heart was first washed with a calcium (Ca²⁺)-free
172 extracellular physiological solution and then with an enzyme-containing solution (Collagenase
173 type IV, Worthington) during 25 to 35 minutes. The free wall, septum and right ventricle were
174 separated, and digestion was stopped with bovine sodium albumin. The tissue was
175 mechanically disrupted with a pipette to release the myocytes. The extracellular Ca²⁺
176 concentration was progressively raised to 1mM.

177 Cardiomyocytes were loaded with the ratiometric Ca²⁺ dye indo-1AM at room temperature
178 during 20 min (2 μM, Life technologies, St-Aubin, France) and cell shortening/Ca²⁺ transients
179 were recorded using electrical-field stimulation (1 Hz, 2 msec, 10V). Experiments were done
180 in Tyrode solution (140 mM NaCl, 4 mM KCl, 1 mM MgCl₂, 20 mM HEPES, 1.8 mM CaCl₂ and
181 11 mM glucose, pH 7.4). Sarcomere length (SL) and fluorescence wavelengths emitted at 405
182 nm (F₄₀₅) and 480 nm (F₄₈₀) were simultaneously recorded using the IonOptix[®] system (Milton,
183 USA) coupled to a Zeiss micro-scope (Zeiss, 40× oil). Data were analyzed using IonWizard 6.6
184 software.

185

186 **Permeabilized cardiomyocytes and mechanics**

187 Permeabilized cardiomyocytes were isolated by mechanical dissociation as described
188 previously¹⁰. The heart was flushed of its blood and the left ventricle was dissected, quickly
189 frozen in liquid nitrogen, and stored at -80°C until use. The day of experiment, about 20 mg of
190 tissue was pre-permeabilized in a relaxing solution at $[Ca^{2+}] = 10^{-9}$ M with anti-protease cocktail
191 (PMSF, Leupeptine, E64) and 1% of Triton X100 within 5 minutes. Tissue was mechanically
192 crushed using a polytron (Ultraturax®) for 2-3 seconds. After filtration, the myocytes were
193 further permeabilized in 0.3% Triton X-100 solution for 6 min at room temperature to remove
194 remaining sarcolemma membranes. After extensive washing with ice-cold relaxing solution,
195 cells were kept on ice and used within the day. Cells were attached to metal tips with an optical
196 glue (NOA 63, North Brunswick, USA) polymerizing under UV light. One tip was linked to a
197 force transducer (AE801, SensoNor, Horten, Norway) allowing to measure developed tension
198 in isometric conditions. The other tip was connected to a piezoelectric motor (ThorLabs Inc,
199 USA) used to shortly modify the length cell for the measure of actin-myosin bridges
200 reformation (kTr). The relationship between Ca^{2+} -activated force and internal Ca^{2+}
201 concentration was measured at two different sarcomere length (SL): 1.9 μ m and 2.3 μ m.
202 Curves were fitted using a modified Hill equation with GraphPad Prism v8.

203

204 **Statistical analysis**

205 Data are presented as mean \pm SEM. Differences were assessed using Student's t-test or Mann
206 Whitney's rank test whenever distribution was not Gaussian after Shapiro-Wilk's normality
207 test. A p-value inferior to 0.05 was considered as significant using GraphPad Prism V9.0
208 software (GraphPad Software, USA). Graphs were realized on GraphPad Prism v9.0.

209

212 References

213

214 1. Thurlbeck WM. Internal surface area and other measurements in emphysema. *Thorax*
215 1967;**22**:483–496.

216 2. Musch TI. Effects of sprint training on maximal stroke volume of rats with a chronic
217 myocardial infarction. *J Appl Physiol* 1992;**72**:1437–1444.

218 3. Teixeira-Coelho F, Fonseca CG, Barbosa NHS, Vaz FF, Souza Cordeiro LM De, Coimbra
219 CC, Pires W, Soares DD, Wanner SP. Effects of manipulating the duration and intensity
220 of aerobic training sessions on the physical performance of rats. *PLoS One* 2017;**12**:1–
221 19.

222 4. Andre L, Fauconnier J, Reboul C, Feillet-Coudray C, Meschin P, Farah C, Fouret G,
223 Richard S, Lacampagne A, Cazorla O. Subendocardial increase in reactive oxygen
224 species production affects regional contractile function in ischemic heart failure.
225 *Antioxidants Redox Signal* 2013;**18**:1009–1020.

226 5. Amancio G de CS, Grabe-Guimarães A, Haikel D, Moreau J, Barcellos NMS,
227 Lacampagne A, Matecki S, Cazorla O. Effect of pyridostigmine on in vivo and in vitro
228 respiratory muscle of mdx mice. *Respir Physiol Neurobiol* 2017;**243**:107–114.

229 6. Chakouri N, Farah C, Matecki S, Amedro P, Vincenti M, Saumet L, Vergely L, Sirvent N,
230 Lacampagne A, Cazorla O. Screening for in-vivo regional contractile defaults to predict
231 the delayed doxorubicin cardiotoxicity in Juvenile Rat. *Theranostics* 2020;**10**:8130–
232 8142.

233 7. Zacchigna S, Paldino A, Falcão-Pires I, Daskalopoulos EP, Dal Ferro M, Vodret S, Lesizza
234 P, Cannatà A, Miranda-Silva D, Lourenço AP, Pinamonti B, Sinagra G, Weinberger F,

- 235 Eschenhagen T, Carrier L, Kehat I, Tocchetti CG, Russo M, Ghigo A, Cimino J, Hirsch E,
236 Dawson D, Ciccarelli M, Oliveti M, Linke WA, Cuijpers I, Heymans S, Hamdani N, Boer
237 M de, Duncker D, Kuster D, Velden J van der, Beauloye C, Bertrand L, Mayr M, Giacca
238 M, Leuschner F, Backs J, Thum T. Toward standardization of echocardiography for the
239 evaluation of left ventricular function in adult rodents: a position paper of the ESC
240 Working Group on Myocardial Function. *Cardiovasc Res* 2020.
- 241 8. Reboul C, Thireau J, Meyer G, André L, Obert P, Cazorla O, Richard S. Carbon
242 monoxide exposure in the urban environment: An insidious foe for the heart? *Respir*
243 *Physiol Neurobiol* 2012;**184**:204–212.
- 244 9. Andre L, Boissière J, Reboul C, Perrier R, Zalvidea S, Meyer G, Thireau J, Tanguy S,
245 Bideaux P, Hayot M, Boucher F, Obert P, Cazorla O, Richard S. Carbon monoxide
246 pollution promotes cardiac remodeling and ventricular arrhythmia in healthy rats. *Am*
247 *J Respir Crit Care Med* 2010;**181**:587–595.
- 248 10. Cazorla O, Szilagyí S, Guennec J Le, Vassort G, Lacampagne A. Transmural
249 stretch-dependent regulation of contractile properties in rat heart and its alteration
250 after myocardial infarction. *FASEB J* 2005;**19**:88–90.

251

252

253 Supplemental Table 1: Plethysmography and lung morphology

	Ctrl	ELA-LPS	p-value
n	13	15	
Ti (msec)	229 ± 10.8	225 ± 8.5	0.767
Te (msec)	403 ± 19	446 ± 22	0.279
TV norm (mL/kg)	4.1 ± 0.13	4.4 ± 0.22	0.311
MV norm (mL/min/g)	0.39 ± 0.02	0.40 ± 0.01	0.910
PIF (mL/s)	14.4 ± 0.7	14.6 ± 0.9	0.808
PEF (mL/s)	9.6 ± 0.4	8.4 ± 0.2*	0.019
Lm (µm)	48 ± 1	68 ± 3*	<0.001

254 Results are presented as mean±SEM. Ti: inspiration time; Te: expiration time; TV: tidal
 255 volume; MV: minute volume; PIF: peak inspiratory flow; PEF: peak expiratory flow
 256 ; Lm: mean linear intercept. *p<0.05. The p-value column corresponds of the comparison
 257 ELA-LPS vs Ctrl.

258

259

260

261

262

263 Supplemental Table 2: *In-vivo* electrical function measured by electrocardiogram telemetry

264 five weeks after the last ELA instillation during a normal activity in their cage.

265

	Ctrl	ELA-LPS	p-value	ELA-LPS + β - blocker
n	17	10		10
HR (bpm)	312.2 \pm 6.6	364.6 \pm 3.8*	<0.001	312.1 \pm 3.5 [†]
PR (msec)	49.6 \pm 0.9	47.46 \pm 0.5	0.474	47.4 \pm 0.4
QRS (msec)	22.6 \pm 0.8	20.9 \pm 0.3	0.675	24.5 \pm 1.1 [†]
QT (msec)	95.7 \pm 1.6	84.5 \pm 1.7*	<0.001	92.4 \pm 1.8 [†]
Dobu Δ HR (bpm)	171 \pm 8.4	88 \pm 11.7*	<0.001	144 \pm 21.4 [†]

266 Results are presented as mean \pm SEM. HR: heart rate (beat per minute); Dobu Δ HR: heart rate

267 variation after dobutamine injection; p<0.05 *ELA-LPS vs Ctrl ; [†]ELA-LPS vs ELA-LPS+ β -

268 blocker. The p-value column corresponds of the comparison ELA-LPS vs Ctrl.

269

270 Supplemental Table 3: *In-vivo* cardiac contractile function five weeks after the last ELA

271 instillation

272

	Ctrl	ELA-LPS	p-value	ELA-LPS + β - blocker
n	22	19		9
LV function				
Heart rate (bpm)	358.5 \pm 5.0	355.6 \pm 6.0	0.712	357.2 \pm 14.9
LVEF (%)	61.7 \pm 1.5	64.0 \pm 1.9	0.334	66.1 \pm 2.4
FS (%)	18.9 \pm 1.4	16.8 \pm 1.1	0.267	19.1 \pm 2.0
CO (mL/min)	132 \pm 5	116 \pm 6*	0.048	112 \pm 5
E (mm/s)	663 \pm 21.7	708 \pm 38.7	0.300	684 \pm 44.5
A (mm/s)	738 \pm 22.3	675 \pm 40.4	0.169	682 \pm 48.2
e' (mm/s)	18.8 \pm 1.7	13.2 \pm 1.0*	0.008	26.7 \pm 4.4 [†]
E/A	0.91 \pm 0.04	1.08 \pm 0.05*	0.015	1.02 \pm 0.06
E/e'	39.3 \pm 2.8	58.2 \pm 5.0*	0.002	34.5 \pm 7.8 [†]
LV morphology				
LVIDd	7.7 \pm 0.2	7.4 \pm 0.1	0.140	6.9 \pm 0.3
LVIDs	3.7 \pm 0.2	3.4 \pm 0.1	0.548	3.1 \pm 0.3
AWT	73.2 \pm 5.1	75.0 \pm 5.2	0.810	81.2 \pm 8.2
PWT	56.9 \pm 4.3	70.4 \pm 7.2	0.098	51.8 \pm 14.0
IVS wall thickening	68.6 \pm 5.3	72.2 \pm 5.9	0.656	66.6 \pm 6.3

RV function

TAPSE (mm)	2.4 ± 0.1	2.6 ± 0.1	0.605	2.6 ± 0.2
S tricuspid (mm/s)	40.2 ± 1.9	40.1 ± 1.8	0.949	42.0 ± 3.3
PET (msec)	69 ± 2.0	68 ± 2.1	0.794	66 ± 3.8

273 Results are presented as mean±SEM. bpm: beat per minute HR: heart rate; LVEF: left
274 ventricular ejection fraction; FS: fractional shortening; CO: cardiac output; E: passive mitral
275 inflow wave; A: active mitral inflow wave; e': early diastolic mitral annular velocity; LVID: left
276 ventricular internal diameter in diastole (d) and systole (s); AWT: anterior wall thickening;
277 PWT: posterior wall thickening; IVS: interventricular septum; TAPSE: tricuspid annular plane
278 systolic excursion; S tricuspid: systolic tricuspid annular velocity; PET: pulmonary ejection
279 time.

280 p<0.05 *ELA-LPS vs Ctrl ; † ELA-LPS vs ELA-LPS+ β-blocker. The p-value column corresponds of
281 the comparison ELA-LPS vs Ctrl.

282

283

284 Supplemental Table 4: Excitation-contraction coupling of intact cardiomyocytes from LV

285

	Ctrl	ELA-LPS	p-value	ELA-LPS + β - blocker
	(n=441/11)	(n=370/9)		(n=197/5)
SL shortening				
diastolic (μm)	1.75 \pm 0.003	1.76 \pm 0.003*	0.0075	1.72 \pm 0.004 [†]
amplitude (%)	11.7 \pm 0.16	12.01 \pm 0.16	0.131	12.3 \pm 0.23
Contraction velocity ($\mu\text{m/s}$)	3.85 \pm 0.06	4.07 \pm 0.07*	0.006	3.30 \pm 0.08 [†]
Relaxation velocity ($\mu\text{m/s}$)	2.56 \pm 0.05	2.77 \pm 0.05*	<0.001	1.89 \pm 0.05 [†]
Ca²⁺ transient				
diastolic	0.763 \pm 0.004	0.783 \pm 0.004*	<0.001	0.798 \pm 0.005 [†]
amplitude	0.272 \pm 0.005	0.307 \pm 0.005*	<0.001	0.277 \pm 0.006 [†]
Tau (ms)	245 \pm 3	234 \pm 3*	0.010	343 \pm 7 [†]

286 Results are presented as mean \pm SEM. (n=number of cells/number of animals); p<0.05 *ELA-287 LPS vs Ctrl [†] ELA-LPS vs ELA-LPS+ β -blocker. The p-value column corresponds of the

288 comparison ELA-LPS vs Ctrl.

289

290

291 Supplemental Table 5: Permeabilized LV cardiomyocytes contractile characteristics

292

	Control	ELA-LPS	p-value	ELA-LPS
			Ctrl vs ELA-LPS	+ β -blocker
	(n=42/5)	(n=47/6)		(n=31/4)
pCa ₅₀	6.07 \pm 0.01	6.03 \pm 0.01*	0.036	6.00 \pm 0.02
nH	3.26 \pm 0.01	3.05 \pm 0.09	0.533	2.81 \pm 0.12 [†]
T _{max} (mN/mm ²)	46.3 \pm 2.0	51.0 \pm 2.2	0.110	47.1 \pm 3.4
T _{passive} (mN/mm ²)	9.72 \pm 0.66	9.53 \pm 0.70	0.546	11.0 \pm 1.9
K _{tr} sub-max (s ⁻¹)	2.43 \pm 0.08	2.01 \pm 0.13*	0.005	2.66 \pm 0.12 [†]
K _{tr} max (s ⁻¹)	6.15 \pm 0.21	5.38 \pm 0.17*	0.014	6.20 \pm 0.18 [†]
Δ pCa ₅₀	0.24 \pm 0.01	0.18 \pm 0.01*	0.006	0.21 \pm 0.02

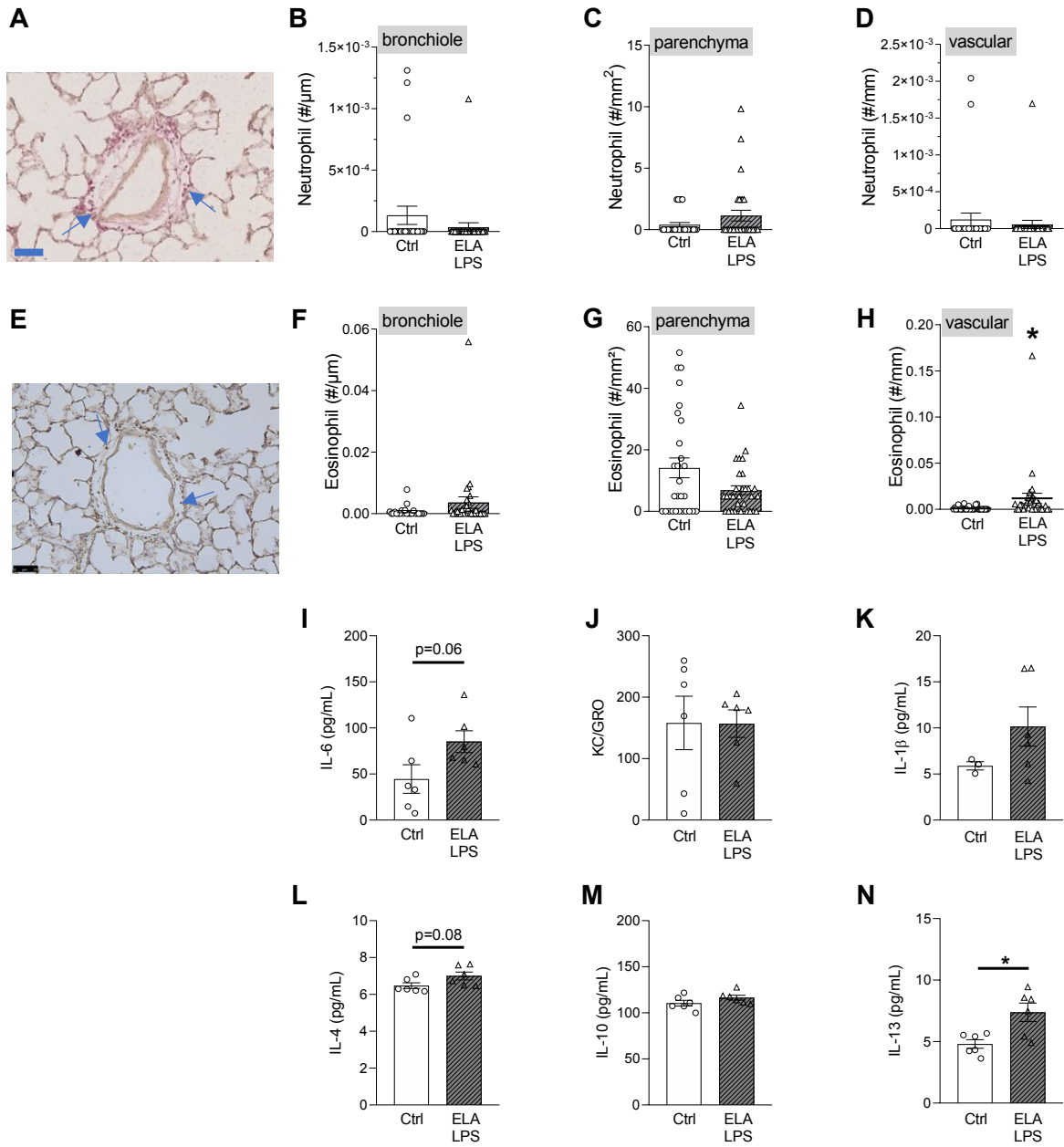
293 Results are presented as mean \pm SEM. (n=number of cells/number of animals); pCa₅₀ Ca²⁺-294 sensitivity of isometric-force production, T_{max} maximum Ca²⁺-activated active tension295 T_{passive} Ca²⁺-independent passive tension, k_{tr},sub-maximal and maximal rate constant of

296 force redevelopment, nH Hill steepness of the force-pCa curve characterizing the

297 cooperativity between myofilament units, p<0.05 *ELA-LPS vs Ctrl [†] ELA-LPS vs ELA-LPS+ β -298 blocker. **The p-value column corresponds of the comparison ELA-LPS vs Ctrl.**

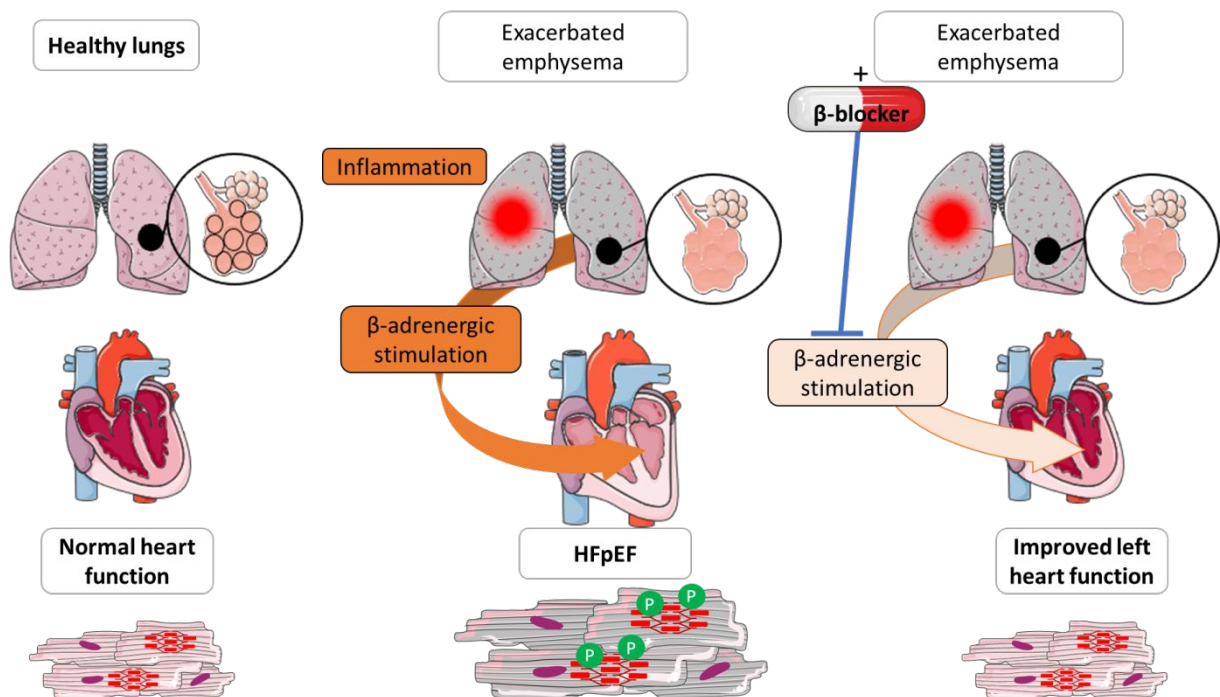
299

Supplemental figures



304 **Supplemental Figure 1: (A-H)** Pulmonary inflammation. Eosinophil **(A)** and neutrophil **(E)**
 305 immunohistochemistry staining on pulmonary sections, X40. White blood count per μm of
 306 bronchiole for neutrophils **(B)** and eosinophils **(F)**; per mm^2 of lung parenchyma for
 307 neutrophils **(C)** and eosinophils **(G)**; per mm of vascular internal diameter for neutrophils **(D)**
 308 and eosinophils **(H)**. (n=4-5 animals/group, 6 areas per animals).
 309 **(I-N)** Systemic plasmatic inflammation cytokines with predominantly T-helper 1 response with
 310 **(I)** Interleukin 6 (IL-6) **(J)** keratinocytes-derived chemokines (KC/GRO) and **(K)** Interleukin-
 311 1beta (IL-1 β) and predominantly T-helper 2 response with **(L)** Interleukin 4 (IL-4), **(M)**
 312 Interleukin-10 (IL-10) and **(N)** Interleukin-13 (IL-13). (n=6 animals per group, duplicate). Data
 313 are represented as mean \pm SEM)

Graphical abstract



319